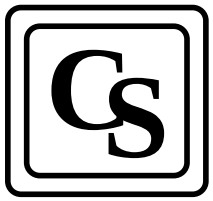

COMPUTER SCIENCE TECHNICAL REPORT

Direct and Adjoint Sensitivity Analysis of Chemical Kinetic Systems with KPP: II – Numerical Validation and Applications

D. Dăescu, A. Sandu,
and G.R. Carmichael

CSTR-02-02
April 2002

Michigan Technological University
1400 Townsend Drive, Houghton, MI 49931

Direct and Adjoint Sensitivity Analysis of Chemical Kinetic Systems with KPP: II – Numerical Validation and Applications

Dacian N. Daescu[†], Adrian Sandu[*], and Gregory R. Carmichael[‡]

[†] Institute for Mathematics and its Applications, University of Minnesota, 400 Lind Hall 207 Church Street S.E. Minneapolis, MN 55455 (daescu@ima.umn.edu).

[*] Department of Computer Science, Michigan Technological University, Houghton, MI 49931 (asandu@mtu.edu).

[‡] Center for Global and Regional Environmental Research, The University of Iowa, Iowa City, IA 52242 (gcarmich@icaen.uiowa.edu).

Abstract

The Kinetic PreProcessor KPP was extended to generate the building blocks needed for the direct and adjoint sensitivity analysis of chemical kinetic systems. An overview of the theoretical aspects of sensitivity calculations and a discussion of the KPP software tools is presented in the companion paper.

In this work the correctness and efficiency of the KPP generated code for direct and adjoint sensitivity studies are analyzed through an extensive set of numerical experiments. Direct decoupled Rosenbrock methods are shown to be cost-effective for providing sensitivities at low and medium accuracies. A validation of the discrete-adjoint evaluated gradients is performed against the finite difference gradients. Consistency between the discrete and continuous adjoint models is shown through step size reduction. The accuracy of the adjoint gradients is measured against a reference gradient value obtained with a standard direct-decoupled method. The accuracy is studied for both constant step size and variable step size integration of the forward model.

Applications of the KPP-1.2 software package to direct and adjoint sensitivity studies, variational data assimilation and parameter identification are considered for the comprehensive chemical mechanism SAPRC-99.

Keywords: sensitivity analysis, data assimilation, parameter identification, optimization.

1 Introduction

Given a chemical kinetics system described by a list of chemical reactions, the Kinetic PreProcessor KPP [9] generates the FORTRAN 77 or C code for the forward model integration and subroutines that allow direct-decoupled/adjoint sensitivity analysis with minimal user intervention. An overview of the theoretical aspects of sensitivity calculations and a discussion of the KPP software tools is presented in the companion paper [26]. In this paper we present an extensive set of numerical experiments and applications of the KPP software to sensitivity studies for chemical kinetics systems.

Our tests use the SAPRC-99 atmospheric chemistry mechanism [4, 5] which considers the gas-phase atmospheric reactions of volatile organic compounds (VOCs) and nitrogen oxides (NOx) in urban and regional settings. The chemical mechanism was developed at University of California, Riverside by Dr. W.P.L. Carter for use in airshed models for predicting the effects of VOC and NOx emissions on tropospheric secondary pollutants formation such as ozone (O3) and other oxidants. In our analysis we consider the condensed fixed-parameter version of the SAPRC-99 mechanism [4] which is suitable for implementation into the Models-3 software framework. This version takes into consideration 211 reactions among 74 variable chemical species (in addition O2, H2, CH4, and H2O concentrations are considered fixed), and is currently incorporated into the three-dimensional regional-scale model STEM-II [2]. A list of the variable chemical species in the model is presented in Table 3.

Hand coding of the forward model and of the direct/adjoint sensitivity models associated with the SAPRC-99 mechanism is a difficult and error prone process. We selected this challenging model to illustrate the ability of the KPP software to implement efficient methods for direct decoupled and adjoint sensitivity analysis.

The paper is organized as follows. In Section 2 we present the numerical solvers available in the KPP library for direct-decoupled and discrete/continuous adjoint sensitivity calculations. Experimental settings, the forward model integration, and issues related to the sparse linear algebra computations are discussed. Direct sensitivity calculations with respect to initial conditions and to reaction rate coefficients using Rosenbrock solvers up to order four are presented in Section 3. The accuracy and the efficiency of the direct-decoupled method is analyzed. Section 4 is dedicated to adjoint sensitivity analysis. Adjoint model validation, consistency between the discrete and adjoint model, and accuracy issues are discussed. The computational expense and the efficiency of the adjoint model are investigated. Applications are presented for time dependent sensitivities with respect to the model state, reaction rate coefficients, and emissions. In Section 5 we present applications of the adjoint modeling to variational data assimilation and parameter estimation using the initial conditions and emission rates as control variables. Concluding remarks and future research directions are presented in Section 6.

2 Numerical Solvers

Rosenbrock methods [19] are well-suited for atmospheric chemistry applications due to their optimal stability properties and conservation of the linear invariants of the system [25]. When the sparsity of the ODE system is carefully exploited, Rosenbrock methods [19] can efficiently integrate atmospheric chemistry systems. The accuracy requirements in atmospheric transport-chemistry models are modest (1%) such that low order methods are usually employed. For the numerical experiments we consider the second-order two-stage L-stable solver ROS2 [31] and the third-order four-stage stiffly accurate solver RODAS3 [25]. An analysis

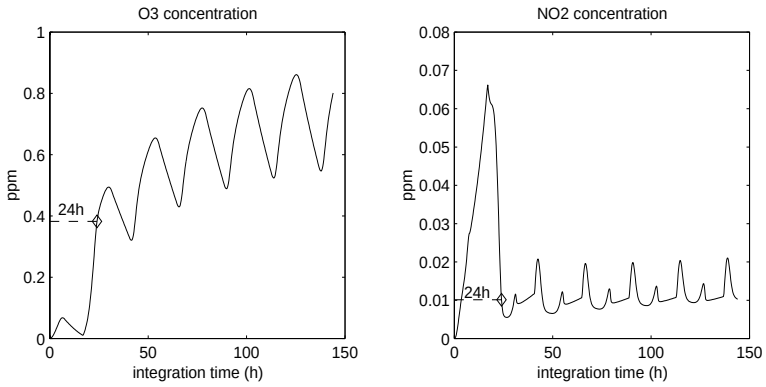

Figure 1: Evolution of O3 and NO2 concentrations. The model state at the end of a 24 hours transient interval (marked with $\diamond$) provides the initial condition for a five days integration run.

of the ROS2 and RODAS3 integration methods plus extensive numerical experiments for chemical models forward integration are presented by Verwer et al. [31] and Sandu et al. [25]. Both integrators use variable step size for error control. For reference, the integration formulae are included in Appendix C. The forward, discrete and continuous adjoint model integrations have been implemented using the KPP software tools. The derivation of the discrete adjoint formulae follows our previous work [7]. Two other methods are included in the KPP-1.2 numerical library: the linearly-implicit Euler method [19] (one-stage Rosenbrock) implemented with constant step size is available in forward/adjoint mode for testing purposes only, and the fourth order four-stage L-stable solver ROS4 [19] is available for direct decoupled sensitivity.

2.1 Experimental Settings

The dynamical model associated with the chemical mechanism is given by a system of nonlinear ordinary differential equations (ODEs)

$$\frac{dy}{dt} = f(y) + E \ , \tag{1}$$

where $y \in R^n$ is the vector of concentrations, $f(y)$ is the chemical production/loss function, and $E \in R^n$ represents the vector of emission rates ($E_i = 0$ if there are no emissions of species i). Throughout this paper an upper index will specify the discrete time moment and a lower index will specify the vector component. For example, y^i is the concentration vector at time t^i and y_j denotes the j^{th} component of the vector y.

For the numerical experiments we selected a pollution scenario with urban VOC and high NO_X levels using input data and reaction rate constants from Carter [4] MD3TEST2, as follows: the model simulation starts at local noon (t^s=12:00 LT) with the concentration of all variable chemical species set to zero. Emissions are prescribed at constant rates for 30 chemical species in the model as specified in Table 4 (E_i^{ref}). We assume a day time interval from 4:30LT (sunrise) to 19:30LT (sunset) with the photolysis reaction rates updated every 15 min, and a constant temperature of $300°K$. The system is integrated for 24 hours (using RODAS3) and the resulting state y^0 at $t^0 = t^s + 24$h is used as the initial state of the model for a five days run. The value y^0 is written to an output file and will serve as input for all numerical experiments performed with various integrators. The one day integration interval is used to avoid initial stiff transients and to allow the system to equilibrate. This process is illustrated in Figure 1 for O3 and NO2 concentrations.

2.2 Sparse Linear Algebra Computations with KPP

For an efficient forward/adjoint integration the sparsity of the ODE system (1) associated with the chemical mechanism must be carefully exploited. The linear algebra computations required during the forward/adjoint integration are efficiently performed using KPP software. The dimension of the state vector of variable chemical species is $n = 74$, but the Jacobian matrix associated with the differential equations system has only 839 nonzero entries out of $74 \times 74 = 5476$ revealing a sparsity of about 85%. KPP selects an optimal ordering of the chemical species such that there are only 920 nonzero entries after the LU matrix decomposition. The KPP ordering of the variable chemical species in the model is presented in Table 3. Since the discrete adjoint model requires Hessian matrices evaluation, it appears that a huge amount of memory must be allocated for Hessian storage. Taking advantage of the symmetry, the full Hessian matrices $H_i = \partial^2 f_i / \partial y^2$, $1 \leq i \leq n$ appear to require $74 \times 74 \times 37 = 202612$ entries to be stored. However, KPP analysis shows that the number of nonzero entries is NHESS = 838, which is less than 0.5% of the previous estimation. The KPP implementation of sparse linear algebra leads to significant computational savings and allows a very efficient forward/adjoint integration.

2.3 Forward Model Integration

Forward model integration is performed with variable step size error control using ROS2 and RODAS3 solvers. Since reaction rates are periodically updated, at each interval $dt = 15$ minutes the integration is restarted with a minimal step size $Hmin = 0.001$s. This may also simulate an operator splitting environment when the chemistry module is incorporated into a 3D atmospheric transport-chemistry model. The evolution of the concentrations during the five days integration from t^0 is shown in Figure 21 (reference run) for representative chemical species from the class of inorganics (O3, NO2, SO2, CO), explicit (HCHO, CCHO, Ethene, Isoprene) and lumped (ALK4, ALK5, ARO1, ARO2) organics, and radicals (OH, HO2, RO2_R, R2O2). The accuracy requirements were given by the absolute tolerance $Atol = 1$ molec/cm^3 and the relative tolerance $Rtol = 10^{-3}$ for all the chemical species in the model. The results obtained with both integrators were within the prescribed accuracy and in Figure 2 we show the relative errors between the predicted concentrations at the end of the five days run when the integration is performed with ROS2 versus RODAS3.

Since the adjoint sensitivity method requires storage of the forward trajectory, it is also of interest to analyze the length of the forward trajectory which is given by the number of steps taken during the forward integration. For the 5 days run, ROS2 required 9970 steps, whereas RODAS3 required only 5115. However, per step RODAS3 is more expensive since it has four internal stages, whereas ROS2 has only two. The distribution of the number of steps on each $[t, t + dt]$ interval displayed in Figure 2 shows that the stiffness of the system increases during the sunrise and sunset transients when a large number of steps needs to be taken.

3 Direct Sensitivity Calculations

We computed the direct sensitivities with respect to initial values and to rate coefficients using ROS2, RODAS3, and ROS4 integration methods. The accuracy of the results and the efficiency of the implementation are compared against a reference solution with the direct-decoupled, off-the-shelf BDF code ODESSA [21], with the tight tolerances $Atol = 1.e-8$ molec/cm^3, $Rtol = 1.e-8$.

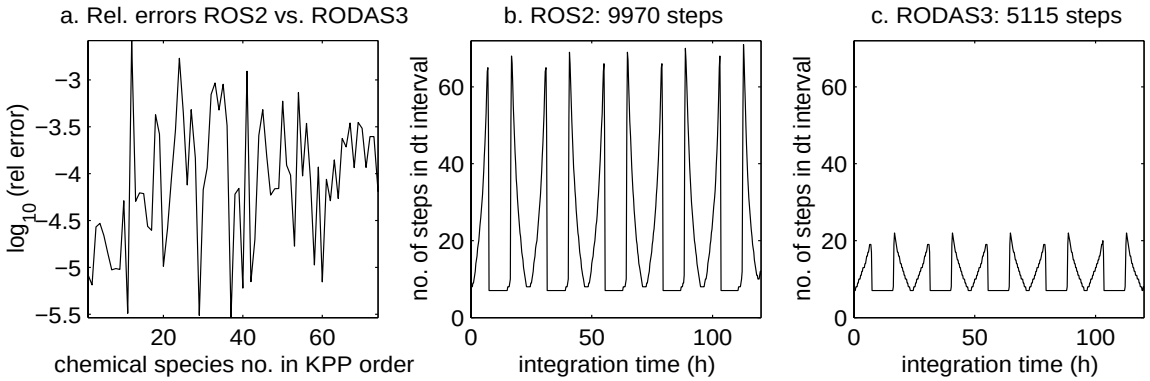

Figure 2: Forward model integration using ROS2 and RODAS3 solvers: (a) ROS2 versus RODAS3 relative differences in the predicted concentrations at $t^{\mathrm{F}} = t^0 + 120h$; (b),(c) Statistics of the number of steps taken in each time interval of length $dt = 15$ min using ROS2 and respectively, RODAS3. A larger number of steps is required during the stiff transients at sunrise and sunset time of the day.

The time evolution of the sensitivity of ozone concentration with respect to its initial value is shown in Figure 3 and the time evolution of the sensitivities of ozone concentration with respect to NO_X initial values in Figure 4.

Direct sensitivities of ozone concentration with respect to six rate coefficients are shown in Figure 5.

ODESSA uses error control for both the concentrations and the sensitivities. We note that setting the proper values of the absolute tolerances for the sensitivities is difficult, since the sensitivity coefficients take values spanning a wide range of magnitudes. For this reason the KPP implementation of Rosenbrock methods only controls the concentration errors. The work-precision diagrams, i.e. the numerical errors versus the CPU time are presented in Figure 6. The ozone concentration errors are shown in the left graphic. The errors of ozone sensitivity at final time with respect to all initial concentrations, i.e.

$$ERR = \sqrt{\frac{1}{NVAR}\sum_{i=1}^{NVAR}\left(\left.\frac{\partial O_3(t^{\mathrm{F}})}{\partial y_i(t^0)}\right|_{\mathrm{numeric}} - \left.\frac{\partial O_3(t^{\mathrm{F}})}{\partial y_i(t^0)}\right|_{\mathrm{reference}}\right)^2}$$

is shown in the right graphic. One notices that sensitivity coefficient errors are of the same order of magnitude as concentration errors. The errors of final concentrations sensitivity with respect to the initial ozone concentration, i.e.

$$ERR = \sqrt{\frac{1}{NVAR}\sum_{i=1}^{NVAR}\left(\left.\frac{\partial y_i(t^{\mathrm{F}})}{\partial O_3(t^0)}\right|_{\mathrm{numeric}} - \left.\frac{\partial y_i(t^{\mathrm{F}})}{\partial O_3(t^0)}\right|_{\mathrm{reference}}\right)^2}$$

are shown in the middle graphic. The results show that some sensitivities are solved inaccurately. Therefore the concentrations-only error control strategy has to be carefully used.

The results of Figure 6 also suggest that direct decoupled Rosenbrock methods are cost-effective (when compared to the BDF sparse code ODESSA) for providing sensitivities at low and medium accuracies. This conclusion parallels the fact that Rosenbrock methods are cost-effective for ODE integration (for calculating concentrations) in the low and medium accuracy range.

The computational times for the forward integration of the model, the direct decoupled sensitivity with respect to all initial conditions and with respect to six rate coefficients are shown in Table 1. The ratios of

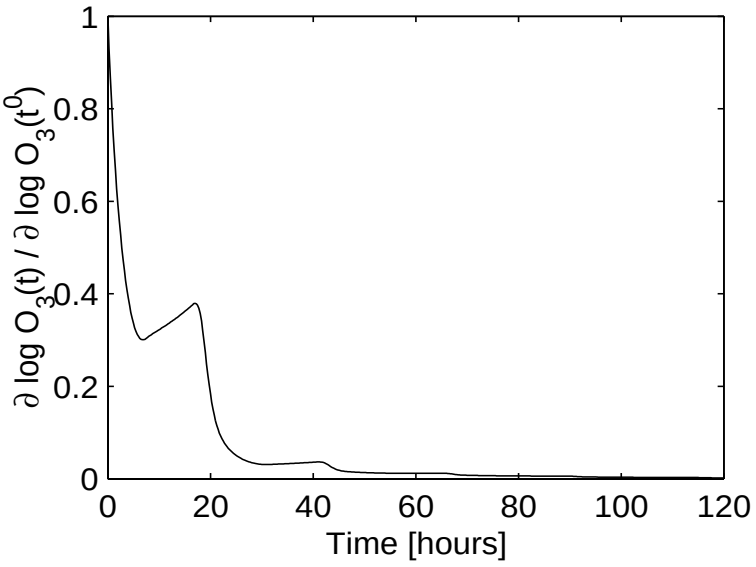

Figure 3: The time evolution of $[O_3](t)$ direct sensitivity with respect to $[O_3](t^0)$.

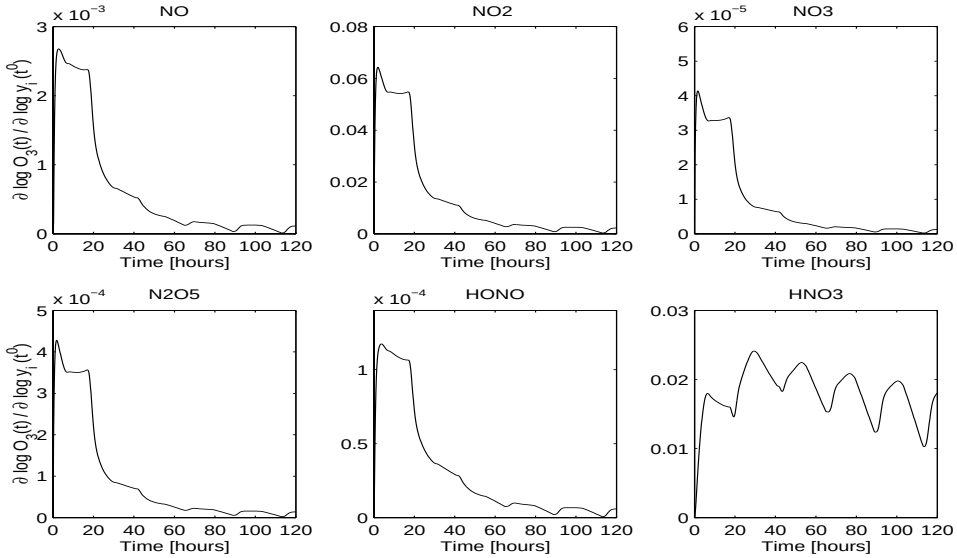

Figure 4: The time evolution of $[O_3](t)$ direct sensitivity with respect to $[NO_X](t^0)$.

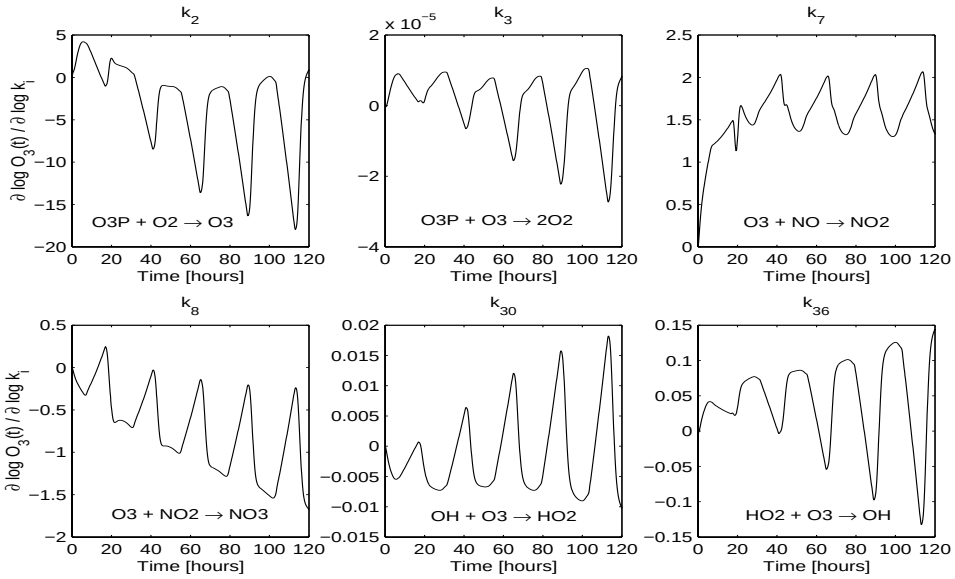

Figure 5: The time evolution of $[O_3](t)$ direct sensitivity with respect to several rate coefficients.

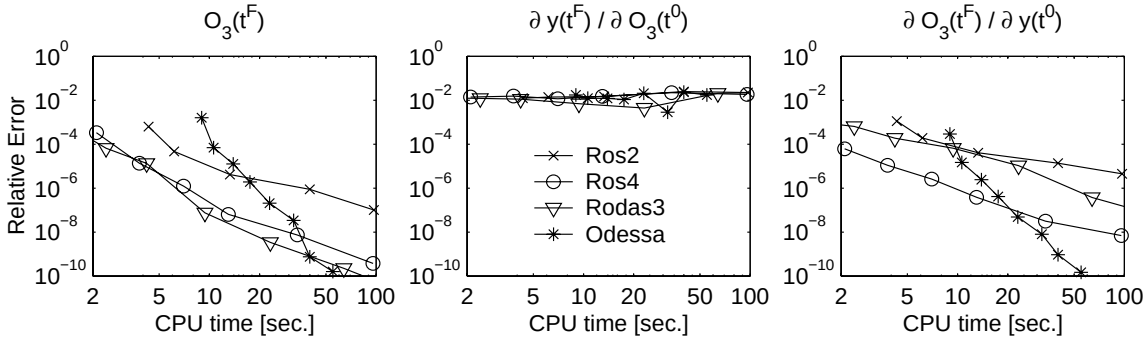

Figure 6: The numerical errors versus CPU time for: $[O_3](t^{\mathrm{F}})$ (left), the direct sensitivity $d[O_3](t^{\mathrm{F}})/dy(t^0)$ (middle), and the direct sensitivity $dy(t^{\mathrm{F}})/d[O_3](t^0)$ (right).

Method	Model	DDM Init. Cond. (NVAR=74)	DDM Rate Coeff. (NCOEFF=6)
Ros2	1.87	73.60 (40)	11.01 (6)
Rodas3	0.66	25.54 (39)	10.36 (15)
Ros4	1.28	78.50 (61)	11.12 (9)
Odessa	2.23	87.82 (40)	21.57 (10)

Table 1: The CPU times (in seconds, on a Pentium III, 1 GHz) for the integration of the forward model, and the integration of the direct decoupled system for sensitivities with respect to all initial values and with respect to six rate coefficients. In parentheses are shown the ratios of DDM times to model integration times.

DDM times to model integration times are sublinear (about half the number of sensitivity coefficients) for sensitivity with respect to initial values. But these ratios are superlinear for the sensitivities with respect to rate coefficients. This can be explained by the overheads due to the analytical calculation of function and Jacobian derivatives with respect to the rate coefficients.

4 Adjoint Sensitivity Analysis

In this section we use the adjoint method to estimate the sensitivity of predicted ozone concentration at the end of the integration interval, $t^{\mathrm{F}} = t^0 + 120\,h$, first with respect to the initial conditions y^0, then with respect to the model state and emissions at intermediate instants in time $t^0 \le t < t^{\mathrm{F}}$. Issues related with validation of the model linearization, consistency between the discrete adjoint and continuous adjoint model, and accuracy of the evaluated gradients are addressed. A comparative study of the discrete (DADJ) versus continuous (CADJ) adjoints is presented for ROS2 and RODAS3 integration methods. The computational expense of the adjoint model is analyzed in terms of memory storage requirements and CPU time relative to the forward model integration.

4.1 Adjoint Model Validation

Since chemical reaction systems are nonlinear, the first problem to address is the validity of the linearization of the model (1). For a given response functional

$$g(u) = g(y(t^{\mathrm{F}}, u)) \tag{2}$$

where $u \in R^m$ is a vector of model parameters, and any perturbation in the input parameters δu, the Taylor series of g at u gives

$$g(u + \delta u) = g(u) + \langle \nabla g(u), \delta u \rangle + o(\|\delta u\|) \tag{3}$$

Therefore, the linear model approximation is satisfied if

$$\lim_{\epsilon \to 0} \frac{g(u + \epsilon \delta u) - g(u)}{\epsilon} = \langle \nabla g(u), \delta u \rangle, \ \forall \delta u \in R^m \tag{4}$$

For practical reasons, since chemical reactions systems are characterized by a wide range of concentrations and roundoff errors may become significant when $\epsilon \to 0$, we will assume that the model linearization is satisfied and the adjoint evaluated gradient is correct if the finite difference approximation

$$\frac{g(u + \epsilon_i e_i) - g(u)}{\epsilon_i} \approx \frac{\partial g(u)}{\partial u_i}, \quad 1 \le i \le m \ , \tag{5}$$

is satisfactory for ϵ_i small enough, where e_i is the i^{th} vector of the canonical base in R^m.

Additional issues must be addressed for the adjoint model validation. The model (1) is nonlinear such that the adjoint model depends on the forward trajectory, which in turn depends on the parameter values. When variable step size integration is performed, the selected steps depend on the parameter values. For a valid test (5) there are two alternatives:

i) perform a constant step size integration;

ii) perform a variable step size integration to evaluate $g(u)$ and store the sequence of the steps taken. Then evaluate $g(u + \epsilon_i e_i)$ using the same sequence of steps.

Using either i) or ii) we may perform a valid test for the *discrete adjoint* model which provides the sensitivity of the *numerically evaluated* response functional with respect to the model parameters. Numerical validation of the continuous adjoint model is more challenging. Since the forward model provides only approximate values of the continuum trajectory, the test (5) for the continuous adjoint gradients can only lead to an agreement within $O(\epsilon) + O(Tol)$, where Tol represents the accuracy of the forward integration. Our approach for the adjoint model validation is to use a constant step size integration to validate the discrete adjoint model, and to show consistency between the discrete and continuous adjoint models through step size reduction. That is, numerically we verify

$$h \searrow 0 \Longrightarrow \|(\nabla g)_{DADJ} - (\nabla g)_{CADJ}\| \searrow 0 \tag{6}$$

We will later use a variable step size integration when we discuss accuracy issues for the evaluated gradients.

4.1.1 Discrete Adjoint Model Validation

We consider the ozone concentration at $t^{\mathrm{F}} = t^0 + 120h$ as the response functional, and the initial conditions as parameters. Therefore, $u = y^0$ and $g(y^0) = [O3](t^{\mathrm{F}}, y^0)$. Sensitivities are evaluated for a constant step size integration $h = 60s$ using ROS2 and RODAS3 solvers. For each solver we compare the discrete adjoint sensitivity against the finite difference approximation (5). Due to the wide range of concentrations, nonlinearity of the system and roundoff errors, finding an optimal perturbation ϵ for the finite difference approximation may be a difficult task requiring extensive trial and error experiments. We consider a perturbation in the initial conditions of 1 part-per-trillion (ppt) for each chemical species at a time, and perform $1 + 74$ runs for the finite difference approximation. For most of the chemical species an agreement of 4 to 6 significant digits is observed between the finite difference and the discrete adjoint gradients, which indicates that the adjoint gradients are properly evaluated. Sensitivity values using finite difference (FD) against discrete adjoint (DADJ) are presented in Table 3 for all chemical species and each numerical solver. In addition, the sensitivities obtained with the continuous adjoint model (CADJ) are also included in Table 3 for each solver. Note that the first eight chemical species in Table 3 are non-reactive and therefore their sensitivity values are zero. For some of the radical species (marked with * in Table 3), we use a perturbation of 10^{-3} ppt to obtain a satisfactory finite difference approximation. Only for the phenoxy radical (BZNO2_O) the finite difference approximation fails to provide reliable results. Since in our model the concentration of BZNO2_O is about 10^{-16} ppt, roundoff errors play a significant role in the finite difference approximation.

From Table 3 it can be seen that although in general we obtained close sensitivity values with different integrators, the accuracy of the forward integration may have a significant impact on the evaluated sensitivities. A good agreement between the finite difference approximation and the discrete adjoint evaluated sensitivities simply implies that the adjoint model was properly implemented. No indication is provided

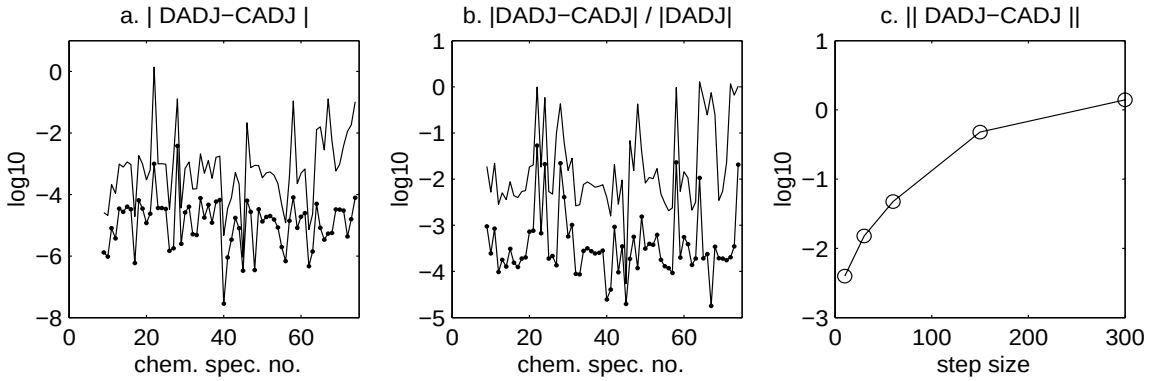

Figure 7: ROS2 discrete versus continuous: (a) absolute and (b) relative differences between the continuous and discrete gradient evaluation with constant step size h=300s (-) and h=10s (.-). (c) Evolution of the Euclidean distance $\|(\nabla g)_{DADJ} - (\nabla g)_{CADJ}\|$ using h=300s, 150s, 60s, 30s, 10s.

on how accurately we estimated *the true* sensitivities given by the exact solution of the forward/adjoint model. For some of the radical species and in particular, for the hydroxyl radical (OH) the discrete adjoint sensitivities we obtained with ROS2 and RODAS3 are quite different. On another hand, the continuous adjoint method applied for each solver offered a consistent sensitivity estimate and we obtained an accurate sensitivity value $\partial[O3](t^{\mathrm{F}})/\partial[OH](t^0) = 0.003891$ with ODESSA package [21] (see also Section 4.2) using the direct decoupled sensitivity method. In Section 2.3 we noticed that even for a modest accuracy of the model integration, a step size as small as a few seconds may be needed during the stiff transients. Since integration with a constant step of a few seconds may not be a practical approach, a variable step size integration with error control is desirable. Before we discuss accuracy issues for the evaluated sensitivities, first we investigate the consistency between the continuous and the discrete adjoint model.

4.1.2 Consistency Between the Discrete and Continuous Adjoint Models

Once a forward integration numerical scheme is selected, the numerical scheme for the discrete adjoint integration is implicitly determined. Hager [18] shows that the discrete adjoint model induced by Runge-Kutta integration schemes may be interpreted as a Runge-Kutta method (usually distinct from the forward method) applied to the continuous adjoint model. Examples of numerical schemes which are consistent with a (forward) equation and whose adjoint is not consistent with the adjoint equation are presented by Sei and Symes [27]. In this section we perform a series of numerical experiments to verify the consistency between the discrete and continuous adjoint model given by relation (6). The continuous adjoint model is integrated backward with the same numerical method and same constant step size used in the forward integration. Experiments are performed using ROS2 and RODAS3 integrators with a decreasing sequence of integration steps: h=300s, 150s, 60s, 30s, and 10s. The absolute and relative differences between the continuous and discrete adjoint gradients when the step size is reduced from 300s to 10s are shown for ROS2 integration in Figure 7 (a),(b), and for RODAS3 integration in Figure 8 (a),(b). The evolution of the distance (6) using the Euclidean norm is shown in Figure 7 (c) for ROS2 and in Figure 8 (c) for RODAS3 and indicates that the convergence (6) is superlinear.

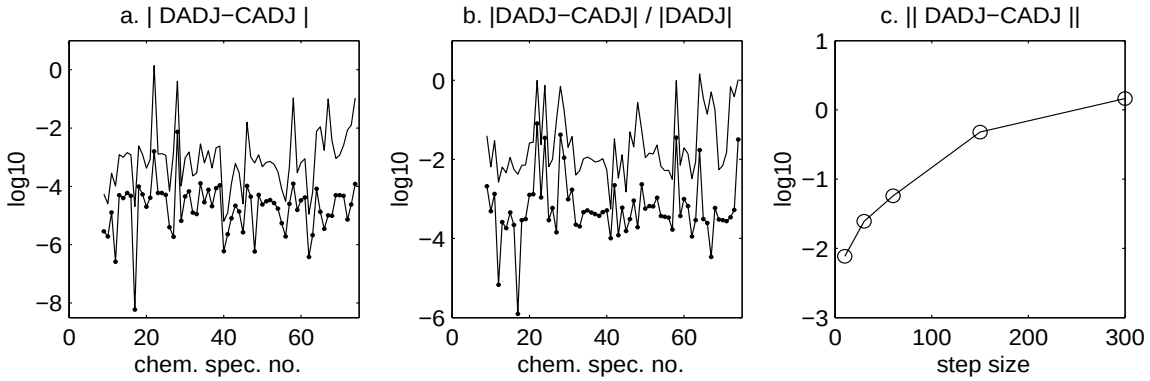

Figure 8: RODAS3 discrete versus continuous: (a) absolute and (b) relative differences between the continuous and discrete gradient evaluation with constant step size h=300s (-) and h=10s (.-). (c) Evolution of the Euclidean distance $\|(\nabla g)_{DADJ} - (\nabla g)_{CADJ}\|$ using h=300s, 150s, 60s, 30s, 10s.

4.2 Accuracy of the Adjoint Sensitivities

In this section we investigate the accuracy of the sensitivities evaluated with the continuous and discrete adjoint models. Reference sensitivity values are obtained by simultaneous solving the ODE system (1) and the associated first-order parametric sensitivity equations using ODESSA code [21] with $Rtol = 10^{-6}$.

We begin our analysis by performing a fixed step size integration, $h = 60s$ of the forward/adjoint model using ROS2 and RODAS3 solvers and comparing the discrete and continuous adjoint sensitivities with the reference values obtained with ODESSA. A graphical illustration of the relative differences of the estimated sensitivity values is shown in Figure 9.

For most components of the state vector, the discrete adjoint approach provided a more accurate sensitivity estimate than the continuous adjoint model. However, the continuous adjoint model appears to provide more robust estimates, whereas large variations in the accuracy estimates may be observed for the discrete adjoint model. In particular, for some of the radical species (see e.g. $TBU\_O, i_{TBU\_O} = 22, O3P, i_{O3P} = 58, OH, i_{OH} = 74$ in Figure 9 and also Table 3) the discrete adjoint estimate was not reliable and the continuous adjoint approach provided accurate values.

4.2.1 Variable Step Size Integration

Variable step size numerical integration of the forward model (1) provides an estimate $\overline{y}(t^i)$ of the true solution $y(t^i)$, $\overline{y}(t^i) = y(t^i) + \delta y(t^i)$, and we may assume that the accuracy requirements of the forward integration are such that $\|\delta y(t^i)\| < Tol$, where Tol is an user prescribed tolerance. Therefore, we only have access to the approximate adjoint model

$$\frac{d\lambda}{dt} = -J^T(t, y + \delta y; p)\lambda \tag{7}$$

$$\lambda(t^{\mathrm{F}}) = \nabla_y g(y(t^{\mathrm{F}}) + \delta y(t^{\mathrm{F}})) \tag{8}$$

which we attempt to solve numerically.

Theoretically, in the continuous adjoint approach the system (7)-(8) may be integrated with its own numerical method and error control. This may not be a practical approach since a dynamical selection of the adjoint step may require frequent forward recomputations. In addition, having available a forward model

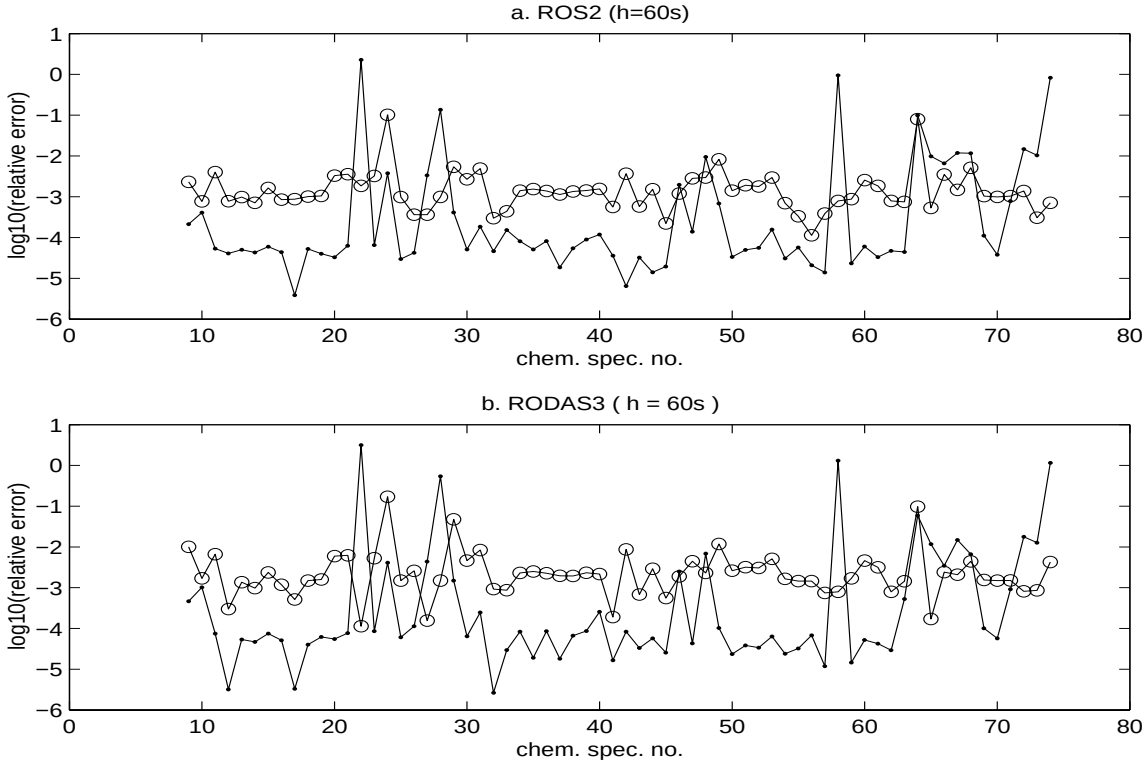

Figure 9: Relative errors for the sensitivity values evaluated using the continuous (o) and discrete (.-) adjoint methods (a) for ROS2 and (b) for RODAS3, with a constant step size h=60s. The reference solution is obtained with ODESSA (Rtol $= 10^{-6}$).

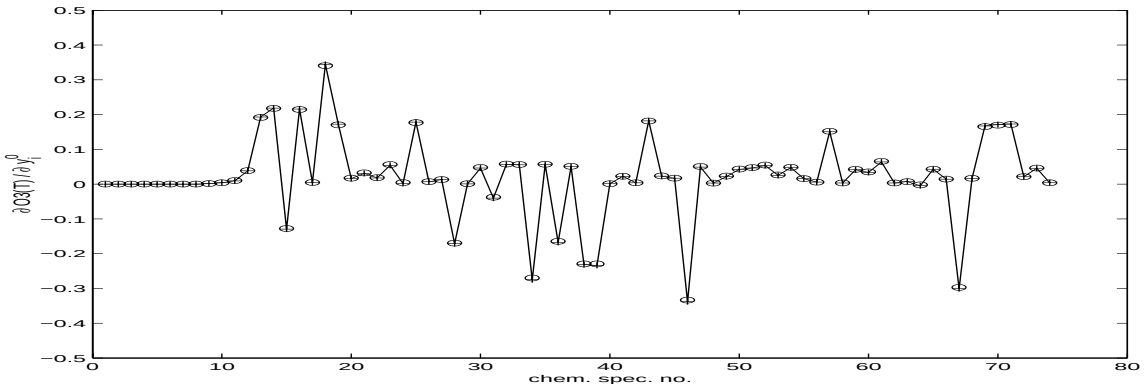

Figure 10: Sensitivity values $\partial[O3](t^{\mathrm{F}})/\partial y_i(t^0)$ obtained with ODESSA (-), discrete adjoint (+) and continuous adjoint ($\circ$) using variable step size RODAS3 integration.

solution such that $\|\delta y(t^i)\| < Tol$ implies that by solving (7)-(8) we may only obtain an estimate $\overline{\lambda} = \lambda + \delta\lambda$ with $\|\delta\lambda\| < C \cdot Tol$, and the constant bound may be quite large. A judicious estimate of how the forward integration errors propagate into the adjoint model is difficult to obtain and significant insight may be gained through a second order sensitivity analysis to evaluate $\partial\lambda/\partial y$. Such analysis is beyond the goal of this paper and we will consider a backward integration of the adjoint model (7)-(8) using the reversed sequence of steps taken during the forward integration.

The discrete adjoint model is induced by the forward integration and may be interpreted as a numerical method applied to the continuous adjoint model. Order reduction of the discrete adjoint for Runge-Kutta integration methods of order three and higher is investigated by Hager [18]. Sei and Symes [27] show that stability and consistency properties are not always preserved by the discrete adjoint model and depend on the numerical integration method.

The forward model (1) is integrated as in Section (2.3) with the tolerances $Atol = 1$ molec/cm^3 , $Rtol = 10^{-3}$, using the variable step size ROS2 and RODAS3 solvers. The reference sensitivity values are obtained with ODESSA. These values and the discrete adjoint model and the continuous adjoint model for the RODAS3 integration are shown in Figure 10. Absolute and relative errors of the discrete and continuous adjoint sensitivities are shown in Figure 11 for ROS2 and in Figure 12 for RODAS3. These results indicate that for each integrator, the discrete adjoint approach provides in general more accurate sensitivity values than the continuous adjoint approach when integration is performed using the reversed step size sequence.

4.3 Computational Expense of the Adjoint Model

The computational expense of the adjoint model is given by the memory resources that need to be allocated for trajectory storage and the CPU time of the gradient evaluation. Intensive research is focused on developing optimal strategies for trajectory storage and checkpointing schemes [16]. Anticipating applications to large scale transport-chemistry models in an operator splitting environment, KPP implements a two-level checkpointing scheme for the forward trajectory storage. The integration interval $[t^0, t^{\mathrm{F}}]$ is uniformly divided in subintervals of length $dt : \mathcal{I}^i_{\rightarrow} = [t^i, t^{i+1}]$, $1 \le i \le I$. The interval length dt is specified by the user, in our experiments $dt = 15$ min. A first forward run from t^0 to t^{F} is used to store the model state at the end of each interval $\mathcal{I}^i_{\rightarrow}$, such that an array of dimension $n \times I$ is stored at this stage. Adjoint (backward) integration in the interval $\mathcal{I}^i_{\leftarrow} = [t^{i+1}, t^i], i = I, 1, -1$ includes a second forward integration in $\mathcal{I}^i_{\rightarrow}$ to store the model

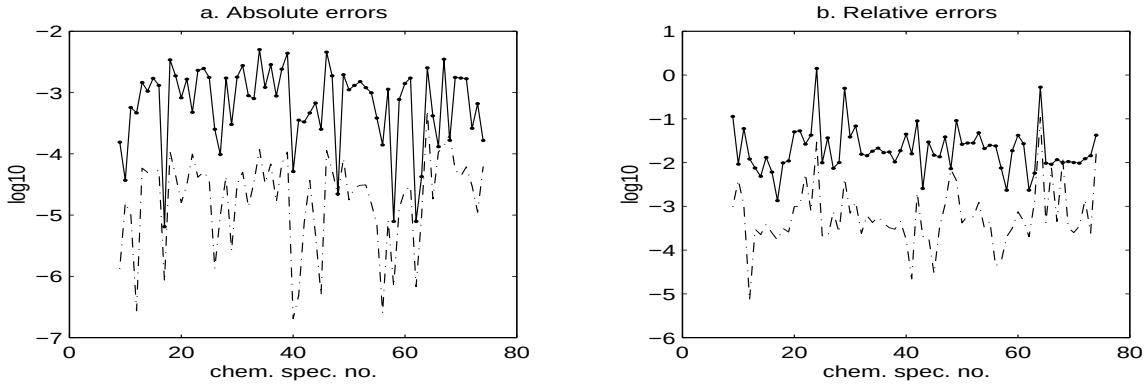

Figure 11: Absolute (a) and relative (b) errors in sensitivity values evaluated with the discrete (dash-dot line) and continuous (solid line with dot) ROS2 adjoint integration with variable step size and forward integration accuracy $Rtol = 0.001$. Adjoint integration is performed using the reversed sequence of steps taken during the forward model integration. The reference sensitivities are obtained with ODESSA.

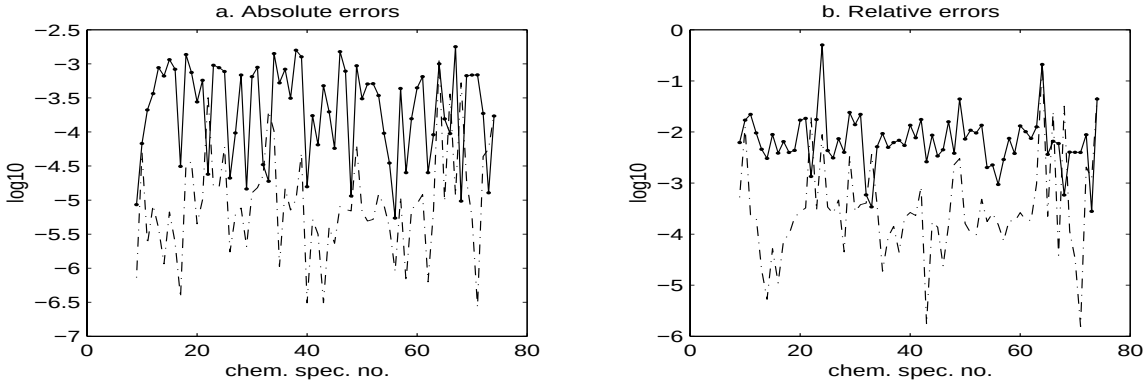

Figure 12: Absolute (a) and relative (b) errors in sensitivity values evaluated with the discrete (dash-dot line) and continuous (solid line with dot) ROS2 adjoint integration with variable step size and forward integration accuracy $Rtol = 0.001$. Adjoint integration is performed using the reversed sequence of steps taken during the forward model integration. The reference sensitivities are obtained with ODESSA.

state after each integration step h_j^i in the $\mathcal{I}_{\rightarrow}^i$ interval. For variable step size integration the sequence of steps taken h_j^i needs also to be stored and the statistics shown in Figure 2 provide insight on the additional state storage requirements during this stage. The pure adjoint (backward) integration is then performed in the interval $\mathcal{I}_{\leftarrow}^i$ and may require some additional forward recomputations of the internal stages of the numerical method at each step. Therefore, the gradient evaluation requires two full forward runs and the pure backward integration.

Griewank [17] has shown that the computational cost of the discrete adjoint code $cpu(DADJ)$ is of the same order as the computational cost of the forward model integration $cpu(FWD)$ (bounded by a factor 5 if no restrictions are considered on the memory access time). Neglecting the cpu time of the forward recomputations, for the continuous adjoint model a ratio $cpu(CADJ)/cpu(FWD) \sim 1$ is desirable using the same numerical method in both the forward and backward integrations. The measured cpu times for pure continuous (CADJ) and discrete (DADJ) adjoint integrations and gradient evaluation (∇g) versus the cpu time of the forward integration (FWD) are shown in Table 2 for ROS2 and RODAS3 integrators using a constant step size forward/backward integration with $h = 60s$. The total cpu time required for gradient evaluation cpu(∇g) includes two forward runs, adjoint integration and the additional overhead introduced by trajectory storage/reload. The results indicate that very efficient implementations for both discrete and continuous adjoint models are obtained using KPP software.

Numerical method	CPU time (sec)						
	FWD	CADJ	CADJ/FWD	$(\nabla g)_{CADJ}$	DADJ	DADJ/FWD	$(\nabla g)_{DADJ}$
RODAS3	1.6	1.9	1.2	5.3	3.7	2.3	7.1
ROS2	1.1	1.2	1.1	3.6	2.1	1.9	4.5

Table 2: CPU time (in seconds) of the forward and adjoint integration with a constant step size h=60s. The gradient time ∇g includes two forward model integrations (FWD), the pure discrete (and respectively continuous) adjoint integration DADJ (CADJ), and additional overhead due to trajectory save/load. Experiments performed on a Pentium III, 930MHz.

A comparative analysis with the direct-decoupled method (Table 1) shows that the adjoint modeling provides a much more efficient approach to evaluate the sensitivity of a scalar response function with respect to a large number of input parameters.

4.4 Time Dependent Sensitivity Analysis

The adjoint method provides an efficient tool for time dependent sensitivity analysis. In this section the adjoint modeling is used to evaluate the sensitivity of ozone concentration $[O3]$ at the end of the integration interval ($t^{\mathrm{F}} = t^0 + 120h$) with respect to the model state at intermediate instants in time and emissions over the time interval $[t^1, t^{\mathrm{F}}], t^0 \leq t^1 < t^{\mathrm{F}}$. Sensitivities with respect to constant and time dependent reaction rates coefficients are also presented; they are obtained at minimal additional cost during the adjoint integration. We initialize the vector $\lambda(t) \in \mathcal{R}^n$ of the adjoint variables associated with the forward model (1) with $\lambda_j(t^{\mathrm{F}}) = 1$ for $j = O3$ and zero for all other components.

4.4.1 Sensitivity to Model State

VOC and NO_X chemistry initiated by reactions with hydroxyl (OH) and respectively, peroxy ($RO2$) radical species is essential to the ozone formation process. The impact on ozone concentration $[O3](t^{\mathrm{F}})$ induced

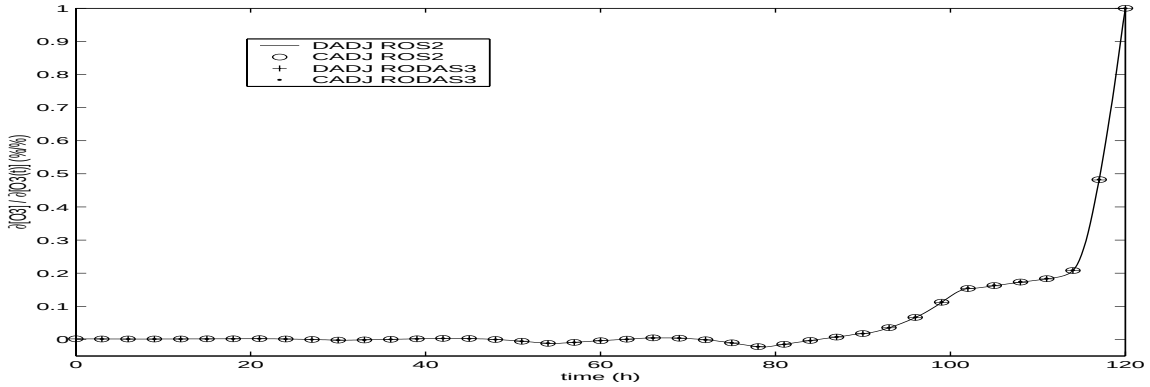

Figure 13: Normalized $[O3](t^F)$ sensitivity with respect to [O3](t), $t^0 \leq t \leq t^F$. Results displayed for continuous and discrete adjoint method using ROS2 and RODAS3 solvers.

by variations in the concentrations of the chemical species in the model at intermediate instants in time $t^0 \leq t < t^F$ may be analyzed by evaluating the time dependent sensitivities

$$s_i(t) = \frac{\partial [O3](t^F)}{\partial y_i(t)} \ , \quad 1 \leq i \leq n \ . \tag{9}$$

Using the adjoint model properties (see [26, Remark 2]), we identify $s_i(t) = \lambda_i(t)$ such that during the adjoint integration to obtain sensitivity with respect to the initial state $\lambda(t^0)$, we obtain at no additional cost the intermediate sensitivities (9). Due to the wide range of concentrations in the chemical system, we consider normalized sensitivity values given by the ratio

$$s_i^*(t) = \frac{\partial \ln([O3](t^F))}{\partial \ln(y_i(t))} = \frac{\partial [O3](t^F)}{\partial y_i(t)} \frac{y_i(t)}{[O3](t^F)} = \frac{y_i(t)}{[O3](t^F)} \lambda_i(t) \ , \quad 1 \leq i \leq n \ , \tag{10}$$

which may be interpreted as the percentual change in the concentration $[O3](t^F)$ due to 1% increase in the concentration of species i at moment t.

We obtained consistent sensitivity trajectories $s_i^*(t), t^0 \leq t < t^F$ within the prescribed accuracy range for both continuous and discrete adjoint approach using variable stepsize (Rtol = 0.001) ROS2 and RODAS3 integration methods as shown in Figure 13 for $s_{O3}^*(t)$.

Note that the sensitivity of ozone concentration at the end of the integration interval is large with respect to ozone state during the previous 24h and it is rapidly diminishing as time moves backward. Therefore, changes in ozone state during the first three days of the integration have little influence on the ozone state at the end of the fifth day. This analysis is also useful for variational data assimilation showing that the length of the assimilation window should be restricted to 1-2 days.

In the same time the adjoint integration provided the sensitivities of ozone with respect to all chemical species in the model. Sensitivity with respect to NO_X species shown in Figure 14 reveals that increasing NO_X concentrations will consistently result in increased ozone formation and the relative impact is highly dependent on the time of the day.

Among the explicit reactive organic product species we found that the impact of variations in the formaldehyde (HCHO) and acetaldehyde (CCHO) concentrations may be significant for the short time evolution of ozone concentrations whereas the ozone relative sensitivity to ethene concentrations is about two orders of magnitude larger than the relative sensitivity with respect to isoprene. These results are shown in Figure 15.

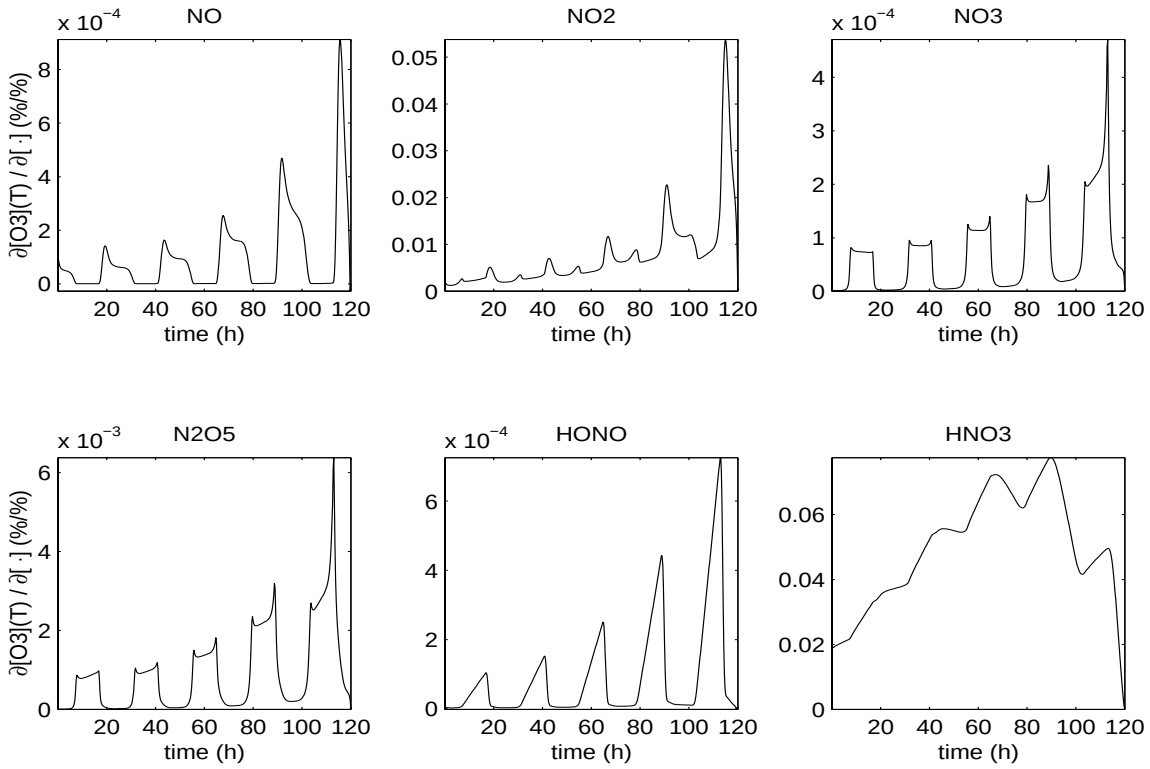

Figure 14: Normalized $[O3](t^F)$ sensitivity with respect to NOx species concentration at intermediate instants in time $t^0 \leq t \leq t^F$.

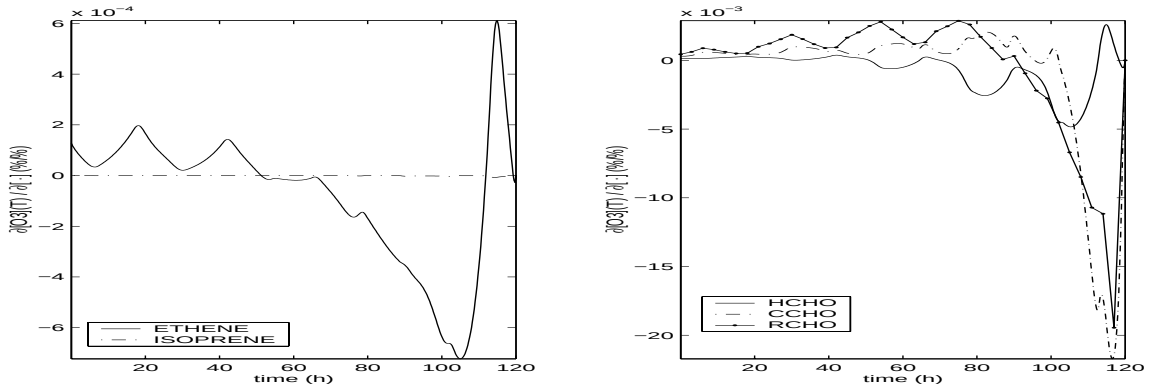

Figure 15: Normalized $[O3](t^F)$ sensitivity with respect to concentrations of reactive organic species explicitly represented in the model at time $t, t^0 \leq t \leq t^F$.

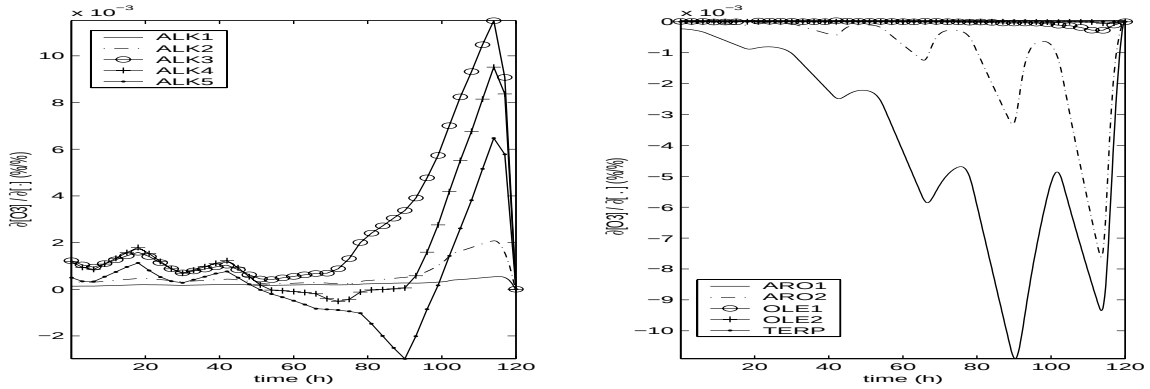

Figure 16: Normalized $[O3](t^F)$ sensitivity with respect to concentrations of lumped parameter species at time $t, t^0 \leq t \leq t^F$.

Relative sensitivities with respect to lumped parameter species displayed in Figure 16 have larger values for alkanes with high OH reactivity (ALK3, ALK4, ALK5) and aromatics (ARO1, ARO2), whereas a small relative sensitivity is shown with respect to alkenes (OLE1, OLE2) and terpenes (TERP).

4.4.2 Sensitivity to Emissions

The impact on ozone formation of various types of emitted VOC is given by the ozone reactivities of the VOC. The "incremental reactivity" (Carter [3]) is given by the partial derivative of ozone with respect to the emissions of the VOC which represents the sensitivity of ozone to VOCs emissions. In this section we study the sensitivity of ozone concentration $[O3]$ at the end of the integration interval ($t^F = t^0 + 120h$) with respect to emissions over the time interval $[t^1, t^F], t^0 \leq t^1 < t^F$. In our model emissions are specified for 30 chemical species at a constant rate E_i as shown in Table 4 (E_i^{ref}). The total amount of VOC emitted in the time interval $[t^1, t^F]$ is given by

$$\mathcal{E}_i(t^1) = \int_{t^1}^{t^F} E_i(t)dt = (t^F - t^1)E_i \tag{11}$$

Using the forward model equation (1), for every emitted chemical species i we have

$$\frac{\partial f_i}{\partial E_i} = 1 \tag{12}$$

such that

$$\frac{\partial [O3](t^F)}{\partial E_i} = \int_{t^1}^{t^F} \lambda_i(t)dt \tag{13}$$

where $\lambda(t) \in \mathcal{R}^n$ denotes the vector of adjoint variables associated with the forward model (1), initialized with $\lambda_j(t^F) = 1$ if $j = O3$ and zero for all other components. The adjoint variables $\lambda_i(t)$ may be interpreted as the sensitivity of the ozone concentration $[O3](t^F)$ with respect to emission rate E_i at time t (see also [26, Remark 2]). From (11) and (13) we obtain the sensitivities

$$s_i(\mathcal{E}, t^1) = \frac{\partial [O3](t^F)}{\partial \mathcal{E}_i(t^1)} = \frac{1}{t^F - t^1} \int_{t^1}^{t^F} \lambda_i(t)dt \tag{14}$$

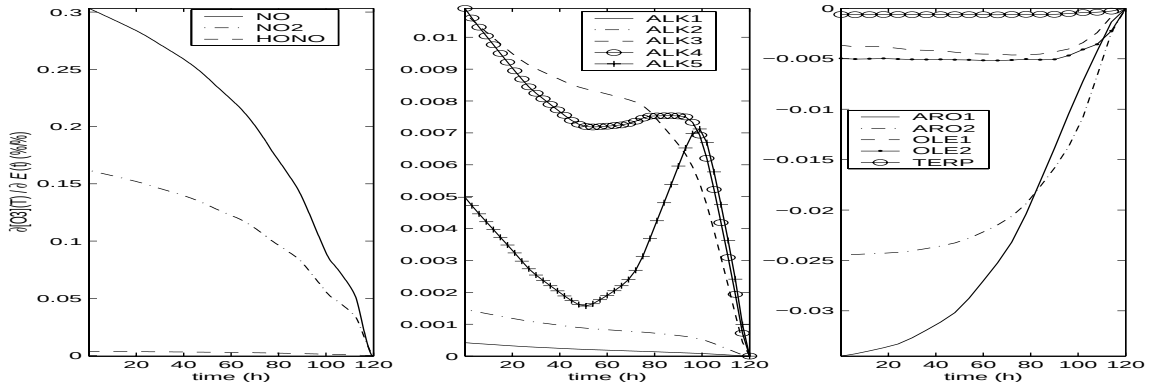

Figure 17: Normalized $[\mathrm{O3}](t^{\mathrm{F}})$ sensitivity with respect to NO_X emissions and lumped parameter species emissions in the time interval $[t, t^{\mathrm{F}}], t^0 \leq t < t^{\mathrm{F}}$

which may be evaluated *simultaneously* for all emission types using *a single* backward integration of the adjoint model. The normalized values

$$s_i^T(\mathcal{E}, t^1) = s_i(\mathcal{E}, t^1)\frac{\mathcal{E}_i(t^1)}{[O3](t^{\mathrm{F}})} \tag{15}$$

indicate the percentual change in ozone concentration corresponding to 1% uniform increase in the emissions of species i over the time interval $[t^1, t^{\mathrm{F}}]$. Normalized sensitivity values with respect to emissions of NO_X and lumped parameter species are shown in Figure 17. Sensitivity values indicate that ozone formation will increase as NO_X and alkanes emissions increase, whereas increasing emissions of aromatics, alkenes and terpenes will inhibit ozone production.

As noted by Carter [3], the incremental reactivity values are highly dependent on the scenario considered and we must emphasize that the results presented in this section are only valid for our particular scenario. Extensive testing is required before general conclusions may be drawn.

4.4.3 Sensitivity to Reaction Rate Coefficients

In this section we use the continuous adjoint model to evaluate the sensitivity of ozone concentration $[\mathrm{O3}](t^{\mathrm{F}})$ with respect to reaction rate coefficients k_j. Chemical reactions in the model are written explicitly as

$$r_j) \quad \sum_{i=1}^{n} s_{i,j}^{-} y_i \xrightarrow{k_j} \sum_{i=1}^{n} s_{i,j}^{+} y_i \ , \quad 1 \leq j \leq R \ , \tag{16}$$

where $s_{i,j}$ are the stoichiometric coefficients. We distinguish between the sensitivity with respect to thermal reactions rate coefficients which in our model are maintained constant, and sensitivity with respect to the photolytical reactions rates which are time dependent.

The sensitivity with respect to constant reaction rates k_j are expressed as

$$s_j(t^1) = \int_{t^1}^{T} \left(\frac{\partial f}{\partial k_j}\right)^T \lambda \, dt \ , \quad t^0 \leq t^1 \leq t^{\mathrm{F}} \tag{17}$$

where

$$\frac{\partial f_i}{\partial k_j} = \left(s_{i,j}^{+} - s_{i,j}^{-}\right) \prod_{i=1}^{n} y_i^{s_{i,j}^{-}} \tag{18}$$

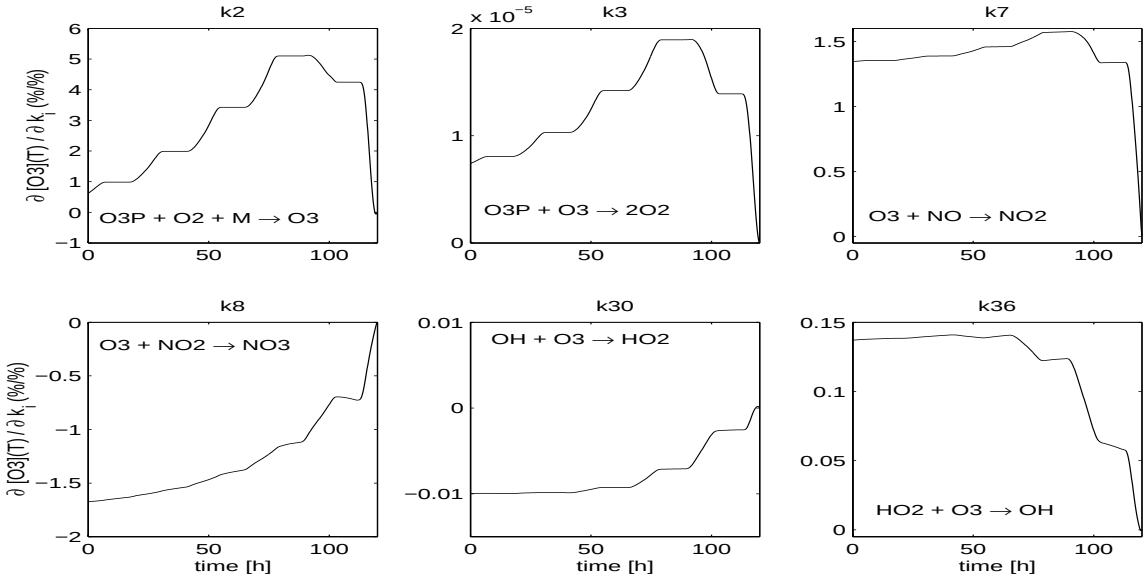

Figure 18: Normalized $[O3](t^{\mathrm{F}})$ sensitivity with respect to constant reaction rate coefficients

and λ is the vector of adjoint variables associated with the state vector y. In Figure 18 we show normalized sensitivity values

$$s_j^*(t^1) = s_j(t^1)\,\frac{k_j}{[O3](t^{\mathrm{F}})} \tag{19}$$

with respect to few of the significant reactions in ozone chemistry.

Remark. The sensitivity values $s_j^*(t^0)$ agree within the prescribed accuracy with the sensitivity values obtained with the direct-decoupled method (see Figure 5 at $t = t^{\mathrm{F}}$).

Sensitivity with respect to instantaneous changes in the photolysis rates at time t^1 are given by

$$s_j(t^1) = \left(\frac{\partial f}{\partial k_j}\right)^T \lambda|_{t=t^1},\ t^0 \le t^1 \le t^{\mathrm{F}} \tag{20}$$

In Figure 19 we show the normalized sensitivity values (20) with respect to the photolysis rates that proved to be most significant in ozone formation.

5 Applications to Variational Data Assimilation

Adjoint modeling is an essential tool for large scale variational data assimilation applications. The variational methods have been extensively used in data assimilation for meteorological and oceanographical models and show promising results for atmospheric chemistry applications [11, 13, 14]. Four dimensional variational data assimilation (4D-Var) searches for an optimal set of model parameters which minimizes the discrepancies between the model forecast and time distributed observational data over the assimilation window. A practical implementation of the minimization process requires a fast and accurate evaluation of the gradient of the cost functional which may be provided by adjoint modeling. A review of the use of the adjoint method in four dimensional atmospheric chemistry data assimilation is presented by Wang et al. [32]. Next we briefly outline the discrete 4D-Var problem formulation and we will refer to Jazwinski [20], Tarantola [30], and

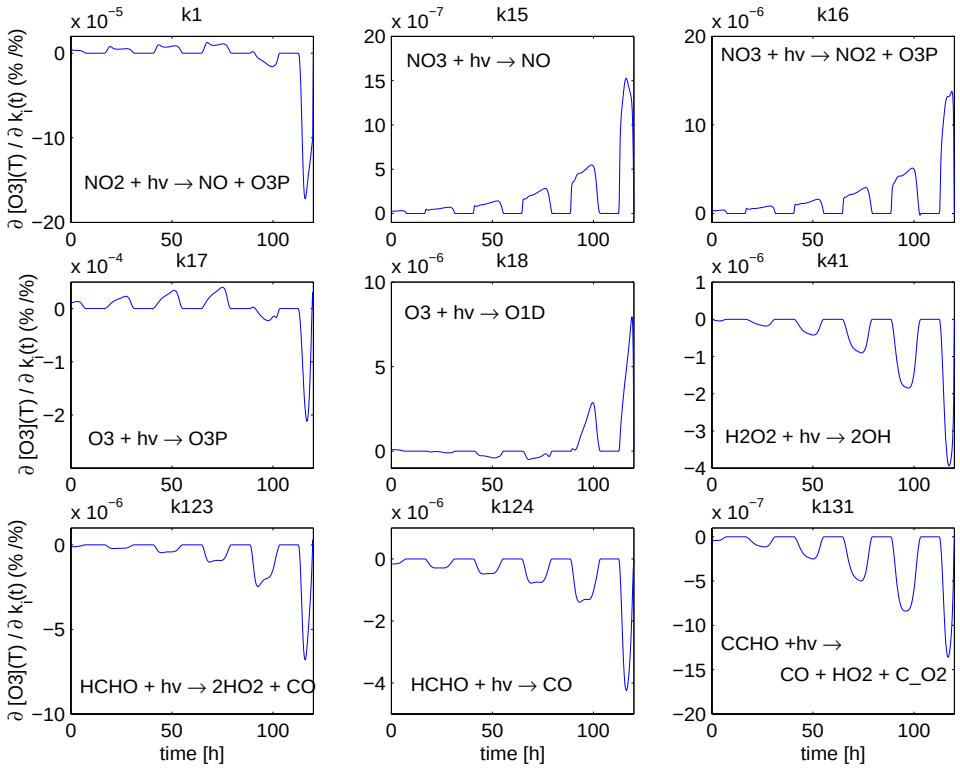

Figure 19: Normalized $[\mathrm{O3}](t^{\mathrm{F}})$ sensitivity with respect to photolysis rate coefficients at time t.

Daley [8] for a complete description of the various assumptions used by the data assimilation techniques, including the continuum formulation and a probabilistic interpretation.

Consider the set of the observations

$$\mathcal{O} = \{\overline{y}^k \in R^{n_k}, 0 \leq k \leq m\} \tag{21}$$

which are taken at discrete moments in time t^k, $0 \leq k \leq m$ over the analysis interval and assume that observations are linearly related with the state

$$\overline{y}^k = H_k y^k + \epsilon^k \ . \tag{22}$$

The observational operator H_k is assumed to be state independent and ϵ^k represents the total observational error which is determined by the measurement error and the error of representativeness (Lorenc [22]). Let u represent the vector of model parameters, and assume that the solution of the model (1) is uniquely determined once the input vector u is specified. Additional information on the model parameters may be taken into account as a "background" estimate u^b of the true parameter values. The 4D variational data assimilation seeks to minimize the discrepancy between the model forecast and observations expressed by the cost function

$$\mathcal{J} = \mathcal{J}^b + \mathcal{J}^o = \frac{1}{2}(u-u^b)^T B^{-1}(u-u^b) + \frac{1}{2}\sum_{k=0}^{m}(H_k y^k - \overline{y}^k)^T R_k^{-1}(H_k y^k - \overline{y}^k) \ . \tag{23}$$

In the probabilistic approach B and R_k represent the covariance matrix of the errors in the background estimate and respectively, observational errors at t^k. Without any probabilistic interpretation, B and R_k are

positive definite diagonal matrices providing appropriate weights for the least squares curve fitting process. By expressing the state vector as a function of parameters, $y^k = y^k(u)$, the 4D-Var problem is formulated

$$\min_u \mathcal{J}(u) \ . \tag{24}$$

In meteorological applications variational techniques are mostly used to find an optimal initial state of the model ($u = y^0$). In atmospheric chemistry modeling uncertainties in various model input parameters (e.g. emission rates, boundary values) must be also considered. For an in-depth analysis of the the adjoint parameter estimation, identifiability issues and regularization techniques in the context of inverse modeling we will refer to Navon [23], Tarantola [30], and Sun [29]. In the numerical experiments presented in this section we investigate the ability of the 4D-Var technique to retrieve the initial model state and provide accurate emission estimates using observational data information. The experiments are performed using the ROS2 solver with variable step size (Rtol = 0.001) and a discrete adjoint model.

5.1 Data Assimilation Framework

The data assimilation procedure is set using the twin experiments method as follows:

Reference run: we start a model run at local noon $t^s = 12{:}00LT$ with the concentration of all variable chemical species set to zero and the "reference" emission rates E_i^{ref} shown in Table 4. The model state obtained after a 24h run at $t^0 = t^s + 24h$ is considered as reference ("true") initial state $(y^0)^{ref}$ of the model for a five days reference run $[t^0, t^0 + 120h]$.

Initial guess run: the experiment is repeated with emission rates increased by 50%, $E_i^{iguess} = 1.5E_i^{ref}$, as shown in Table 4. The model state obtained after a 24h run at $t^0 = t^s + 24h$ is considered as "initial guess" model state for a five days forecast run using E_i^{iguess} as emission rates.

Observations and assimilation window: We consider a 24h assimilation window $[t^0, t^0 + 24h]$. No observations are provided for radical species (marked with $\diamond$ in Table 3). For all other chemical species in the model concentrations obtained during the reference run are provided as hourly observations starting from $t^0 + 1h$.

Parameters: the control parameters are the concentration of variable chemical species at t^0 (dimension 74) and the emission rates (dimension 30), $u = (y^{0T}, E^T)^T$.

Cost functional: We assume that information to the data assimilation process is provided only by the "observations" such that no background term is included in the cost functional (23). To achieve a better scaling and to eliminate the positivity constraint, we consider $\ln u$ as control variables and the logarithmic form of the cost functional

$$\mathcal{J}(\ln u) = \frac{1}{2} \sum_{k=1}^{24} \sum_{i \in \mathcal{O}^k} [(\ln y_i^k - \ln \overline{y}_i^k]^2 \tag{25}$$

where $\mathcal{O}_k$ represents the set of components of the state vector observed at t^k.

Optimization algorithm: Quasi-Newton limited memory L-BFGS [1]. The optimization proceeds until the cost functional is reduced to 0.01% of its initial value.

5.2 Numerical Results

Using data assimilation we aim to provide an accurate estimate of the "true" initial model state $(y^0)^{ref}$ and emission rates E_i^{ref} such that an improved forecast is obtained for a five days model run. In the data assimilation process information provided by the observations is propagated to all the variables of the model.

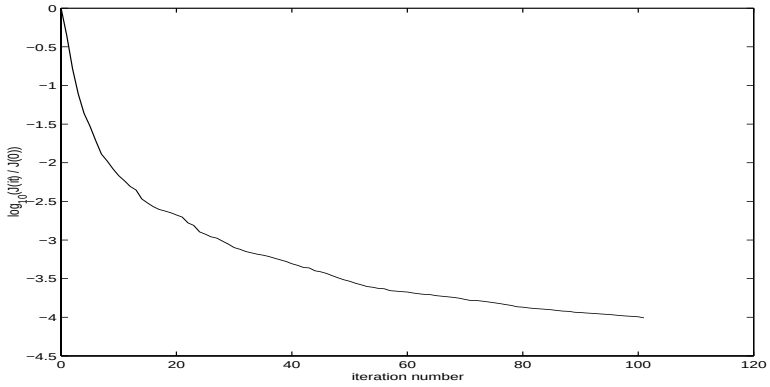

Figure 20: Evolution on a log10 scale of the normalized cost functional during the minimization process.

Chemical interactions among the model variables may allow the assimilation process to provide an improved forecast not only for the observed components of the state vector, but also for the chemical species for which observations are not available. Therefore, we further investigate the ability of the data assimilation to provide an accurate estimate of the evolution of the concentrations of radical species for which no observations were provided.

The reference run, the initial guess forecast, the assimilation results and the forecast after the assimilation process takes place are shown in Figure 21 for various chemical species. By performing data assimilation, not only we have obtained an accurate representation of the model state evolution in the assimilation window [0,24] h, but also an accurate forecast was obtained for the full five days period. An accurate evolution of the concentrations of the radical species was also obtained. Emission rates estimates E_i^{assim} displayed in Table 4 show that using the assimilation procedure the "true" emission rate values were successfully retrieved.

The evolution of the normalized cost functional (25) during the minimization process is shown in Figure 20. The convergence process is fast during the first 30 iterations when the cost functional is reduced to less than 0.1% of its initial value, whereas further reduction to 0.01% requires more than 70 additional iterations. Faster convergence may be achieved through a better scaling of the cost functional components [6] or by using Hessian information which may be efficiently provided by a second order adjoint model (LeDimet et al. [10]).

6 Conclusions and Future Work

In this paper we presented an extensive set of numerical experiments and applications of the new Kinetic PreProcessor release KPP-1.2 to direct decoupled and adjoint sensitivity analysis. Our results indicate that KPP may be used as a flexible and efficient tool to generate code for sensitivity studies of the chemical reactions mechanisms. We illustrated KPP abilities by selecting a challenging test model, the state-of-the-science gas-phase chemical mechanism SAPRC-99. For this comprehensive model implementation of the direct decoupled sensitivity method and hand generation of the adjoint code may be a difficult, time consuming, and error prone task.

Issues related with model linearization, accuracy, consistency, and computational expense of the discrete and adjoint model were addressed. The new direct decoupled Rosenbrock methods we proposed have been shown to be cost-effective for providing sensitivities at low and medium accuracies. In addition, particular

properties of the Rosenbrock methods may be exploited for the adjoint modeling [7]. By taking full advantage of the sparsity of the chemical mechanism, the KPP software generates efficient discrete and continuous adjoint models.

The comparative study of discrete versus continuous adjoints has shown that the continuous adjoint model offers more flexibility, is computationally less expensive, and provides more robust results than the discrete adjoint model. The discrete adjoint model however produces more accurate sensitivity values.

We should emphasize that the efficiency of the KPP software relies on its particular design for chemical kinetics systems and KPP is not a general purpose adjoint modeling tool as TAMC [15] or Odyssée [24]. Generating the discrete adjoint model associated with sophisticated numerical integrators is a complex task and an efficient implementation requires in-depth knowledge of the numerical scheme and forward mode computations. For this reason, the use of discrete adjoints in atmospheric chemistry applications has been limited to explicit or low order linearly implicit numerical methods. For efficiency, a hand generated discrete adjoint code was often implemented [12, 11]. Currently, KPP provides discrete adjoint implementation of the linearly implicit Euler, ROS2, and RODAS3 solvers, whereas the continuous adjoint model may be integrated with any user selected numerical method. As our research advances, new solvers from the class of Runge-Kutta methods will be included in discrete adjoint mode.

Adjoint modeling has various applications and few of them were illustrated in this paper: backward and time dependent sensitivity analysis, parameter estimation, and data assimilation. Model reduction of chemical kinetics [28] is an important field which we will investigate in our future work using direct/adjoint sensitivity analysis. By providing efficient operations involving Hessian matrices, KPP software may be also used to obtain second order information which may be applied to sensitivity analysis and data assimilation [10].

An efficient implementation of the chemistry module into comprehensive 3D transport-chemistry models is essential as computations involving chemical transformations may require as much as 90% of the total cpu time. Applications of adjoint modeling to atmospheric chemistry represent a new research direction which is growing at a fast peace and the KPP software tools can be used to facilitate the efficient forward/adjoint model integration.

Acknowledgements

The work of A. Sandu was supported in part by NSF CAREER award ACI-0093139.

References

[1] R. Byrd, P. Lu, and J. Nocedal. A limited memory algorithm for bound constrained optimization. *SIAM J. Sci. Stat. Comput.*, 16(5):1190–1208, 1995.

[2] G.R. Carmichael, L.K. Peters, and T. Kitada. A second generation model for regional-scale transport/ chemistry/ deposition. *Atmospheric environment*, 20:173–188, 1986.

[3] W.P.L. Carter. Development of ozone reactivity scales for volatile organic compounds. *J. Air & Waste Manage. Assoc.*, 44:881–899, 1994.

[4] W.P.L. Carter. Implementation of the SAPRC-99 Chemical Mechanism into the Models-3 Framework. Technical report, Report to the United States Environmental Protection Agency, January 2000.

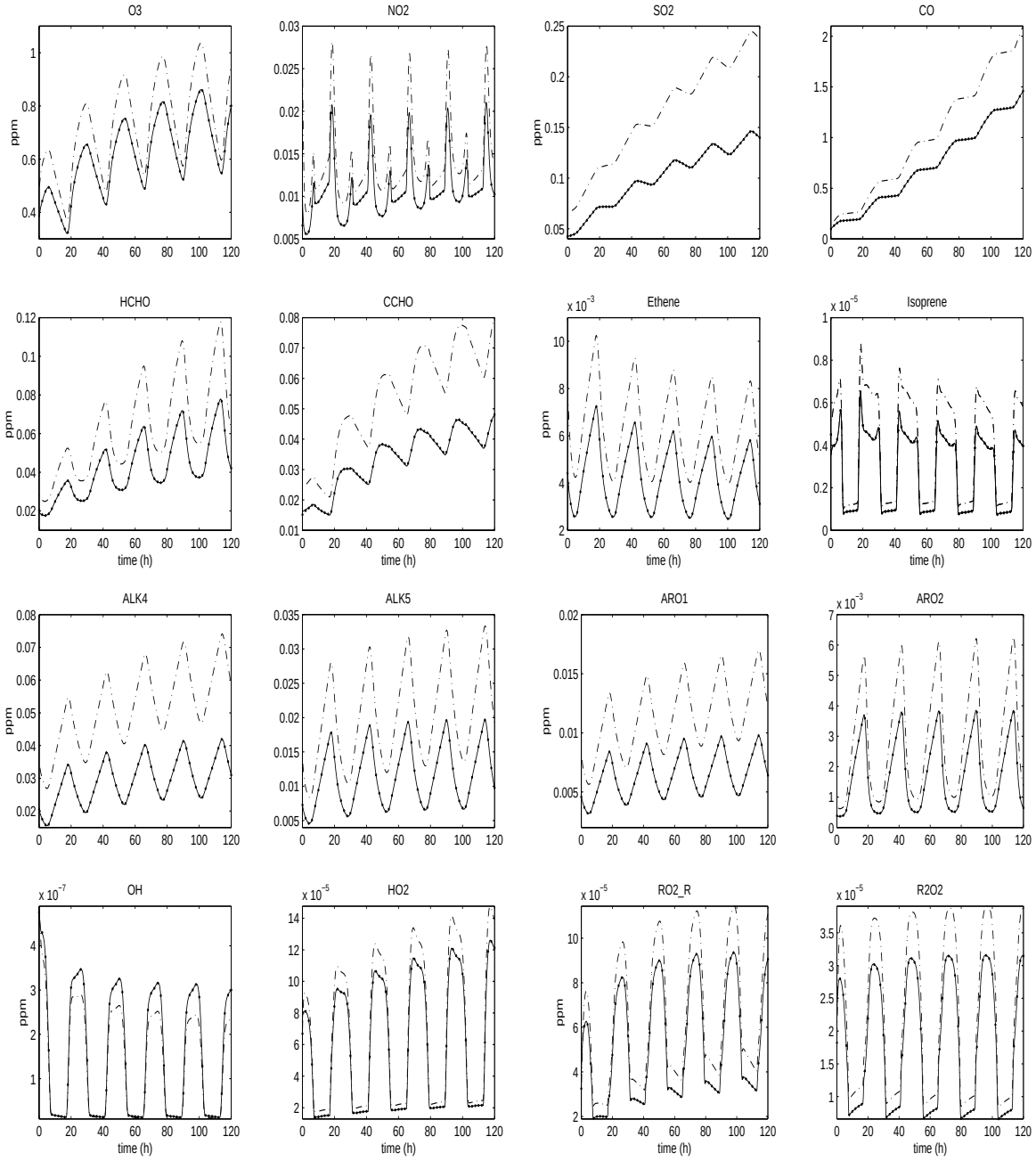

Figure 21: Evolution of the concentrations for a five days forecast. Trajectories are shown for chemical species representing the class of inorganics (O3, NO2, SO2, CO), explicit (HCHO, CCHO, Ethene, Isoprene) and lumped (ALK4, ALK5, ARO1, ARO2) organics, and radicals (OH, HO2, RO2_R, R2O2). Reference run with continuous line, initial guess run with dashdot line, assimilation run with solid dots. Data assimilation is performed over a 24h assimilation window [0 24]h.

[5] W.P.L. Carter. Documentation of the SAPRC-99 Chemical Mechanism for VOC Reactivity Assessment. Technical Report No. 92-329, and 95-308, Final Report to California Air Resources Board Contract, May 2000.

[6] W.C. Chao and L.-P. Chang. Development of a four-dimensional variational analysis system using the adjoint method at gla. part 1: Dynamics. *Mon. Weath. Rev.*, 120:1661–1673, 1992.

[7] D. Daescu, G.R. Carmichael, and A. Sandu. Adjoint implementation of Rosenbrock methods applied to variational data assimilation problems. *Journal of Computational Physics*, 165(2):496–510, 2000.

[8] R. Daley. *Atmospheric Data Analysis.* Cambridge University Press, 457pp, 1991.

[9] V. Damian-Iordache, A. Sandu, M. Damian-Iordache, G. R. Carmichael, and F. A. Potra. The Kinetic Preprocessor KPP - A Software Environment for Solving Chemical Kinetics. submitted to Computers and Chemical Engineering, 2001.

[10] F.-X. Le Dimet, I.M. Navon, and D.N. Daescu. Second order information in data assimilation. *Mon. Weath. Rev.*, 130(3):629–648, 2002.

[11] H. Elbern and H. Schmidt. A four-dimensional variational chemistry data assimilation for Eulerian chemistry transport model. *Journal of Geophysical Research*, 104(D15):18,583–18,598, 1999.

[12] H. Elbern, H. Schmidt, and A. Ebel. Variational data assimilation for tropospheric chemistry modeling. *Journal of Geophysical Research*, 102(D13):15,967–15,985, 1997.

[13] Q. Errera and D. Fonteyn. Four-dimensional variational chemical assimilation of crista stratospheric measurements. *J. Geophys. Res.*, 106-D11:12,253–12,265, 2001.

[14] M. Fisher and D. J. Lary. Lagrangian four-dimensional variational data assimilation of chemical species. *Q.J.R. Meteorol. Soc.*, 121:1681–1704, 1995.

[15] R. Giering and T. Kaminski. Recipes for adjoint code construction. *Recipes for Adjoint Code Construction*, 1998.

[16] A. Griewank. Achieving logarithmic growth of temporal and spatial complexity in reverse automatic differentiation. *Optimization methods and software*, 1:35–54, 1992.

[17] A. Griewank. Evaluating Derivatives: Principles and Techniques of Algorithmic Differentiation. *Frontiers in Applied Mathematics*, 19, 2000.

[18] W. W. Hager. Runge-kutta methods in optimal control and the transformed adjoint system. *Numerische Mathmatik*, 87:247–282, 2000.

[19] E. Hairer and G. Wanner. *Solving Ordinary Differential Equations II. Stiff and Differential-Algebraic Problems.* Springer-Verlag, Berlin, 1991.

[20] A.H. Jazwinski. *Stochastic Processes and Filtering Theory.* Academic Press, 376pp, 1970.

[21] J.R. Leis and M.A. Kramer. ODESSA - An Ordinary Differential Equation Solver with Explicit Simultaneous Sensitivity Analysis. *ACM Transactions on Mathematical Software*, 14(1):61, 1986.

[22] A. C. Lorenc. Analysis methods for numerical weather prediction. *Q.J.R. Meteorol. Soc.*, 112:1177–1194, 1986.

[23] I.M. Navon. Practical and theoretical aspects of adjoint parameter estimation and identifiability in meteorology and oceanography. *Dynamics of Atmospheres and Oceans. Special Issue in honor of Richard Pfeffer*, 27(1–4):55–79, 1998.

[24] N. Rostaing, Dalmas, and A. S., Galligo. Automatic differentiation in odyssée. *Tellus*, 45:558–568, 1993.

[25] A. Sandu, J. G. Blom, E. Spee, J. G. Verwer, F.A. Potra, and G.R. Carmichael. Benchmarking stiff ODE solvers for atmospheric chemistry equations II - Rosenbrock Solvers. *Atmospheric Environment*, 31:3459–3472, 1997.

[26] A. Sandu, D. Daescu, and G.R. Carmichael Direct and Adjoint Sensitivity Analysis of Chemical Kinetic Systems with KPP: I – Theory and Software Tools. Submitted to Atmospheric Environment, 2002.

[27] A. Sei and W. Symes. A note on consistency and adjointness for numerical schemes. Technical Report CRPC-TR95527, Department of Computational and Applied Mathematics, Rice University, 1995.

[28] B. Sportisse and R. Djouad. Reduction of chemical kinetics in air pollution modeling. *Journal of Computational Physics*, 164:354–376, 2000.

[29] Ne-Zheng Sun. *Inverse Problems in Groundwater Modeling.* Kluwer Academic Publishers, 337pp, 1994.

[30] A. Tarantola. *Inverse Problem Theory: Methods for Data Fitting and Model Parameter Estimation.* Elsevier Science Publishers, 613pp, 1987.

[31] J. Verwer, E.J. Spee, J. G. Blom, and W. Hunsdorfer. A second order Rosenbrock method applied to photochemical dispersion problems. *SIAM Journal on Scientific Computing*, 20:1456–1480, 1999.

[32] Wang, K.Y. , Lary, D.J., Shallcross, D.E., Hall S.M., and Pyle J.A. A review on the use of the adjoint method in four-dimensional atmospheric-chemistry data assimilation. *Q.J.R. Meteorol. Soc.*, 127(576 (Part B)):2181–2204, 2001.

A Comparison of Different Methods for Gradient Computation

Table 3 shows the gradients $\partial O3(t^{\mathrm{F}})/\partial y_i^0$ evaluated using finite differences (FD), discrete adjoints (DADJ) and continuous adjoints of RODAS3 and ROS2 solvers with h=60s. Chemical species in the model are listed in KPP selected order. Non-reactive species in the model are marked with † and radicals are marked with $^\diamond$. A perturbation $\epsilon = 1ppt$ was used in the finite difference approximation. For chemical species marked with * we used $\epsilon = 0.001ppt$.

KPP	Chemical	RODAS3			ROS2		
No.	species	FD	DADJ	CADJ	FD	DADJ	CADJ
1†	H2SO4	0.00000E+00	0.00000E+00	0.00000E+00	0.00000E+00	0.00000E+00	0.00000E+00
2†	HCOOH	0.00000E+00	0.00000E+00	0.00000E+00	0.00000E+00	0.00000E+00	0.00000E+00
3†	CCO_OH	0.00000E+00	0.00000E+00	0.00000E+00	0.00000E+00	0.00000E+00	0.00000E+00
4†	RCO_OH	0.00000E+00	0.00000E+00	0.00000E+00	0.00000E+00	0.00000E+00	0.00000E+00
5†	CCO_OOH	0.00000E+00	0.00000E+00	0.00000E+00	0.00000E+00	0.00000E+00	0.00000E+00
6†	RCO_OOH	0.00000E+00	0.00000E+00	0.00000E+00	0.00000E+00	0.00000E+00	0.00000E+00
7†	XN	0.00000E+00	0.00000E+00	0.00000E+00	0.00000E+00	0.00000E+00	0.00000E+00
8†	XC	0.00000E+00	0.00000E+00	0.00000E+00	0.00000E+00	0.00000E+00	0.00000E+00
9	SO2	0.13782E-02	0.13782E-02	0.13914E-02	0.13779E-02	0.13779E-02	0.13808E-02
10$^\diamond$	O1D	0.39652E-02	0.39653E-02	0.39626E-02	0.39710E-02	0.39710E-02	0.39663E-02
11	ALK1	0.95137E-02	0.95138E-02	0.95762E-02	0.95135E-02	0.95136E-02	0.95512E-02
12	BACL	0.38263E-01	0.38264E-01	0.38252E-01	0.38265E-01	0.38265E-01	0.38234E-01
13	PAN	0.19317E+00	0.19317E+00	0.19292E+00	0.19317E+00	0.19317E+00	0.19299E+00
14	PAN2	0.21875E+00	0.21875E+00	0.21854E+00	0.21875E+00	0.21875E+00	0.21860E+00
15	PBZN	-0.12949E+00	-0.12949E+00	-0.12919E+00	-0.12949E+00	-0.12949E+00	-0.12929E+00
16	MA_PAN	0.21605E+00	0.21605E+00	0.21581E+00	0.21605E+00	0.21605E+00	0.21588E+00
17	H2O2	0.47951E-02	0.47951E-02	0.47927E-02	0.47951E-02	0.47951E-02	0.47909E-02
18	N2O5	0.34423E+00	0.34424E+00	0.34373E+00	0.34423E+00	0.34423E+00	0.34390E+00
19	HONO	0.17247E+00	0.17247E+00	0.17221E+00	0.17248E+00	0.17248E+00	0.17231E+00
20	ALK2	0.16202E-01	0.16202E-01	0.16297E-01	0.16202E-01	0.16202E-01	0.16254E-01
21	ALK3	0.31035E-01	0.31035E-01	0.31226E-01	0.31034E-01	0.31034E-01	0.31143E-01
22$^{\diamond *}$	TBU_O	0.74430E-01	0.74434E-01	0.17916E-01	0.58709E-01	0.58702E-01	0.17881E-01
23	ALK5	0.54248E-01	0.54248E-01	0.54530E-01	0.54247E-01	0.54247E-01	0.54419E-01
24	ARO2	0.17430E-02	0.17433E-02	0.20331E-02	0.17424E-02	0.17427E-02	0.19140E-02
25	HNO4	0.17847E+00	0.17847E+00	0.17822E+00	0.17848E+00	0.17848E+00	0.17831E+00
26	COOH	0.68350E-02	0.68350E-02	0.68520E-02	0.68345E-02	0.68345E-02	0.68367E-02
27$^\diamond$	HOCOO	0.13174E-01	0.13171E-01	0.13111E-01	0.13159E-01	0.13157E-01	0.13109E-01
28$^{\diamond *}$	BZNO2_O	-0.59814E+00	-0.17698E+00	-0.17093E+00	-0.33906E+00	-0.19449E+00	-0.17102E+00
29	MEOH	0.60444E-03	0.60445E-03	0.63238E-03	0.60379E-03	0.60380E-03	0.60682E-03
30	ALK4	0.46236E-01	0.46237E-01	0.46447E-01	0.46236E-01	0.46236E-01	0.46357E-01
31	ARO1	-0.40153E-01	-0.40152E-01	-0.39826E-01	-0.40155E-01	-0.40154E-01	-0.39965E-01
32	DCB2	0.56868E-01	0.56868E-01	0.56921E-01	0.56871E-01	0.56871E-01	0.56885E-01
33	DCB3	0.55593E-01	0.55592E-01	0.55642E-01	0.55603E-01	0.55602E-01	0.55618E-01
34	CRES	-0.27493E+00	-0.27494E+00	-0.27433E+00	-0.27493E+00	-0.27494E+00	-0.27458E+00
35	DCB1	0.56370E-01	0.56370E-01	0.56510E-01	0.56372E-01	0.56372E-01	0.56456E-01
36	NPHE	-0.16736E+00	-0.16736E+00	-0.16700E+00	-0.16736E+00	-0.16736E+00	-0.16714E+00
37	ROOH	0.50228E-01	0.50228E-01	0.50325E-01	0.50228E-01	0.50228E-01	0.50284E-01

Table 3: Finite difference (FD), discrete adjoint (DADJ) and continuous adjoint (CADJ) evaluated gradients $\partial O3(t^{\mathrm{F}})/\partial y_i^0$ using RODAS3 and ROS2 solvers with h=60s.

KPP	Chemical	RODAS3			ROS2		
No.	species	FD	DADJ	CADJ	FD	DADJ	CADJ
38	BALD	-0.23158E+00	-0.23158E+00	-0.23114E+00	-0.23158E+00	-0.23158E+00	-0.23128E+00
39	PHEN	-0.23380E+00	-0.23381E+00	-0.23328E+00	-0.23380E+00	-0.23381E+00	-0.23350E+00
40	CO	0.11600E-02	0.11600E-02	0.11622E-02	0.11599E-02	0.11599E-02	0.11579E-02
41	MGLY	0.22371E-01	0.22371E-01	0.22375E-01	0.22371E-01	0.22372E-01	0.22358E-01
42	ACET	0.37252E-02	0.37252E-02	0.37579E-02	0.37255E-02	0.37255E-02	0.37392E-02
43	HNO3	0.18192E+00	0.18192E+00	0.18180E+00	0.18192E+00	0.18192E+00	0.18182E+00
44	ETHENE	0.22913E-01	0.22913E-01	0.22979E-01	0.22912E-01	0.22912E-01	0.22947E-01
45	GLY	0.16976E-01	0.16976E-01	0.16985E-01	0.16975E-01	0.16975E-01	0.16971E-01
46$^{\diamond}$	BZ_O	-0.33741E+00	-0.33742E+00	-0.33763E+00	-0.33759E+00	-0.33761E+00	-0.33787E+00
47	ISOPRENE	0.48924E-01	0.48925E-01	0.49140E-01	0.48929E-01	0.48929E-01	0.49060E-01
48$^{\diamond}$	R2O2	0.29810E-02	0.29821E-02	0.29958E-02	0.29740E-02	0.29744E-02	0.29939E-02
49	TERP	0.21421E-01	0.21420E-01	0.21670E-01	0.21434E-01	0.21432E-01	0.21595E-01
50	METHACRO	0.42481E-01	0.42481E-01	0.42591E-01	0.42481E-01	0.42481E-01	0.42540E-01
51	OLE1	0.46460E-01	0.46460E-01	0.46606E-01	0.46461E-01	0.46461E-01	0.46547E-01
52	ISOPROD	0.53388E-01	0.53388E-01	0.53549E-01	0.53389E-01	0.53389E-01	0.53481E-01
53	OLE2	0.25213E-01	0.25213E-01	0.25340E-01	0.25215E-01	0.25215E-01	0.25286E-01
54	MVK	0.47508E-01	0.47508E-01	0.47585E-01	0.47508E-01	0.47509E-01	0.47540E-01
55	CCHO	0.15508E-01	0.15508E-01	0.15530E-01	0.15509E-01	0.15509E-01	0.15513E-01
56	HCHO	0.58214E-02	0.58214E-02	0.58295E-02	0.58211E-02	0.58211E-02	0.58217E-02
57	RNO3	0.15063E+00	0.15063E+00	0.15074E+00	0.15063E+00	0.15063E+00	0.15069E+00
58$^{\diamond *}$	O3P	0.78351E-02	0.78358E-02	0.33817E-02	0.66128E-02	0.66127E-02	0.33817E-02
59	RCHO	0.41519E-01	0.41519E-01	0.41589E-01	0.41520E-01	0.41520E-01	0.41555E-01
60	MEK	0.33771E-01	0.33771E-01	0.33925E-01	0.33771E-01	0.33771E-01	0.33856E-01
61	PROD2	0.63755E-01	0.63755E-01	0.63953E-01	0.63754E-01	0.63755E-01	0.63871E-01
62	O3	0.33846E-02	0.33846E-02	0.33820E-02	0.33845E-02	0.33845E-02	0.33820E-02
63$^{\diamond *}$	HO2	0.72890E-02	0.72897E-02	0.72830E-02	0.72946E-02	0.72939E-02	0.72881E-02
64$^{\diamond *}$	RO2_N	-0.44712E-02	-0.44706E-02	-0.42890E-02	-0.42812E-02	-0.42823E-02	-0.43715E-02
65$^{\diamond *}$	MA_RCO3	0.42230E-01	0.42230E-01	0.42726E-01	0.42313E-01	0.42313E-01	0.42711E-01
66$^{\diamond}$	C_O2	0.14321E-01	0.14331E-01	0.14347E-01	0.14283E-01	0.14286E-01	0.14331E-01
67$^{\diamond *}$	BZCO_O2	-0.29611E+00	-0.29611E+00	-0.29996E+00	-0.29701E+00	-0.29702E+00	-0.30014E+00
68$^{\diamond}$	RO2_R	0.16698E-01	0.16644E-01	0.16608E-01	0.16755E-01	0.16727E-01	0.16619E-01
69	NO	0.16740E+00	0.16740E+00	0.16715E+00	0.16740E+00	0.16740E+00	0.16724E+00
70	NO2	0.17118E+00	0.17118E+00	0.17093E+00	0.17118E+00	0.17118E+00	0.17102E+00
71	NO3	0.17286E+00	0.17284E+00	0.17273E+00	0.17287E+00	0.17286E+00	0.17282E+00
72$^{\diamond *}$	CCO_O2	0.20829E-01	0.20830E-01	0.21189E-01	0.20893E-01	0.20893E-01	0.21177E-01
73$^{\diamond *}$	RCO_O2	0.45071E-01	0.45072E-01	0.45693E-01	0.45181E-01	0.45181E-01	0.45668E-01
74$^{\diamond *}$	OH	-0.63646E-03	-0.63446E-03	0.38750E-02	0.67029E-03	0.67080E-03	0.38888E-02

Table 3: (continued) Finite difference (FD), discrete adjoint (DADJ) and continuous adjoint (CADJ) evaluated gradients $\partial O3(t^{\mathrm{F}})/\partial y_i^0$ using RODAS3 and ROS2 solvers with h=60s.

B Emissions

Chemical species	Emission Rate (ppm/min)				
	E_i^{ref}	E_i^{iguess}	$\lvert(E_i^{ref} - E_i^{iguess})/E_i^{ref}\rvert$	E_i^{assim}	$\lvert(E_i^{ref} - E_i^{assim})/E_i^{ref}\rvert$
NO	6.944E-05	10.416E-05	0.5	6.934E-05	0.00130
NO2	3.472E-05	5.208E-05	0.5	3.474E-05	0.00071
HONO	6.944E-07	1.041E-06	0.5	6.947E-07	0.00053
SO2	3.472E-05	5.208E-05	0.5	3.462E-05	0.00260
ETHENE	1.312E-05	1.968E-05	0.5	1.315E-05	0.00238
ISOPRENE	3.007E-07	4.510E-07	0.5	3.007E-07	0.00019
TERP	5.694E-07	8.541E-07	0.5	5.693E-07	0.00005
MEOH	4.089E-06	6.134E-06	0.5	4.087E-06	0.00060
HCHO	7.786E-06	1.168E-05	0.5	7.869E-06	0.01059
CCHO	1.608E-06	2.412E-06	0.5	1.856E-06	0.15447
RCHO	1.195E-06	1.793E-06	0.5	1.301E-06	0.08800
GLY	8.431E-08	1.264E-07	0.5	9.072E-08	0.07612
MGLY	5.815E-08	8.722E-08	0.5	6.497E-08	0.11743
METHACRO	9.008E-07	1.351E-06	0.5	9.012E-07	0.00044
ISOPROD	6.201E-08	9.302E-08	0.5	6.153E-08	0.00780
BALD	5.217E-08	7.825E-08	0.5	5.356E-08	0.02666
ACET	3.522E-06	5.283E-06	0.5	3.697E-06	0.04974
MEK	2.264E-06	3.397E-06	0.5	2.372E-06	0.04753
PROD2	1.340E-06	2.010E-06	0.5	1.352E-06	0.00946
PHEN	4.206E-07	6.310E-07	0.5	4.207E-07	0.00016
CRES	3.888E-07	5.832E-07	0.5	3.870E-07	0.00452
ALK1	8.103E-06	1.215E-05	0.5	8.179E-06	0.00938
ALK2	1.306E-05	1.959E-05	0.5	1.306E-05	0.00049
ALK3	3.259E-05	4.888E-05	0.5	3.254E-05	0.00126
ALK4	2.893E-05	4.340E-05	0.5	2.889E-05	0.00165
ALK5	2.123E-05	3.185E-05	0.5	2.123E-05	0.00033
ARO1	8.185E-06	1.227E-05	0.5	8.201E-06	0.00202
ARO2	6.070E-06	9.106E-06	0.5	6.069E-06	0.00021
OLE1	7.209E-06	1.081E-05	0.5	7.197E-06	0.00165
OLE2	5.538E-06	8.307E-06	0.5	5.535E-06	0.00048

Table 4: Reference (E_i^{ref}), initial guess (E_i^{iguess}), and data assimilation (E_i^{assim}) estimated emission rates.

C Rosenbrock Solvers

Consider the autonomous initial value problem

$$\dot{y} = f(y) \ , \quad y(t^0) = y_0.$$

An s-stage Rosenbrock method (Hairer et al., 1991) provides a numerical time discretization of the initial value problem using the formulas

$$y^{n+1} = y^n + \sum_{i=1}^{s} b_i k_i, \tag{26}$$

$$k_i = hf(y^n + \sum_{j=1}^{i-1} \alpha_{ij} k_j) + hJ \sum_{j=1}^{i} \gamma_{ij} k_j, \tag{27}$$

Different Rosenbrock methods are defined by their coefficients α_{ij}, γ_{ij}, and b_i. A different set of weights $\tilde{b}_i$ is sometimes used to compute a secondary solution $\tilde{y}$, such that the difference $y^{n+1} - \tilde{y}^{n+1}$ offers an estimate of the numerical error.

Ros-2 is a 2-stage, order 2 method with coefficients:

$$(\alpha_{ij}) = \begin{pmatrix} 0 & \\ 1 & 0 \end{pmatrix}, \quad (\gamma_{ij}) = \begin{pmatrix} 1+\sqrt{2}/2 & \\ 1 & 1+\sqrt{2}/2 \end{pmatrix}, \quad (b_i) = \begin{pmatrix} 1/2 & 1/2 \end{pmatrix} \ .$$

Rodas-3 is a 4-stage, order 3 embedded pair with coefficients:

$$(\alpha_{ij}) = \begin{pmatrix} 0 & & & \\ 0 & 0 & & \\ 1 & 0 & 0 & \\ 3/4 & -1/4 & 1/2 & 0 \end{pmatrix}, \quad (\gamma_{ij}) = \begin{pmatrix} 1/2 & & & \\ 1 & 1/2 & & \\ -1/4 & -1/4 & 1/2 & \\ 1/12 & 1/12 & -2/3 & 1/2 \end{pmatrix},$$

and weights

$$(b_i) = \begin{pmatrix} 5/6 & -1/6 & -1/6 & 1/2 \end{pmatrix}, \quad (\tilde{b}_i) = \begin{pmatrix} 3/4 & -1/4 & 1/2 & 0 \end{pmatrix}.$$